

**Supporting Information:**

**Self-consistent calculation of localized orbital  
scaling correction for correct electron densities  
and energy level alignment in density  
functional theory**

Yuncai Mei,<sup>†</sup> Zehua Chen,<sup>†</sup> and Weitao Yang<sup>\*,†,‡</sup>

<sup>†</sup>*Department of Chemistry, Duke University, Durham, North Carolina 27708, USA*

<sup>‡</sup>*Department of Physics, Duke University, Durham, North Carolina 27708, USA*

E-mail: weitao.yang@duke.edu

## I. Supplemental results for SCF-LOSC

### 1. Molecular dissociation

If not specified, below are the calculation details for cases of molecular dissociation studied in this work. All the DFT calculation are performed from using an in-house developed QM<sup>4</sup>D package,<sup>S1</sup> if not specified. The MRCI+Q calculation is performed from using GAMESS package.<sup>S2,S3</sup> The GW calculation is performed from using FHI-aims package.<sup>S4,S5</sup> The MP2 and the D3 version of Grimme's dispersion with Becke-Johnson damping (D3BJ) are performed from using Gaussian 16 package.<sup>S6</sup> cc-pVTZ is used as the basis set for all the calculations. For LOSC calculations, aug-cc-pVTZ-RIFIT is used as the fitting basis set in the

construction of LOSC curvature matrix. The molecular geometries for 1,4-benzenediamine and tetracyanoethylene (TCNE) are optimized from using B3LYP/6-31g\* with Gaussian 16 package.<sup>S6</sup> In the following text, the D-A complex refers to the 1,4-benzenediamine/TCNE complex system. The donor molecule refers to 1,4-benzenediamine and the acceptor refers to TCNE.

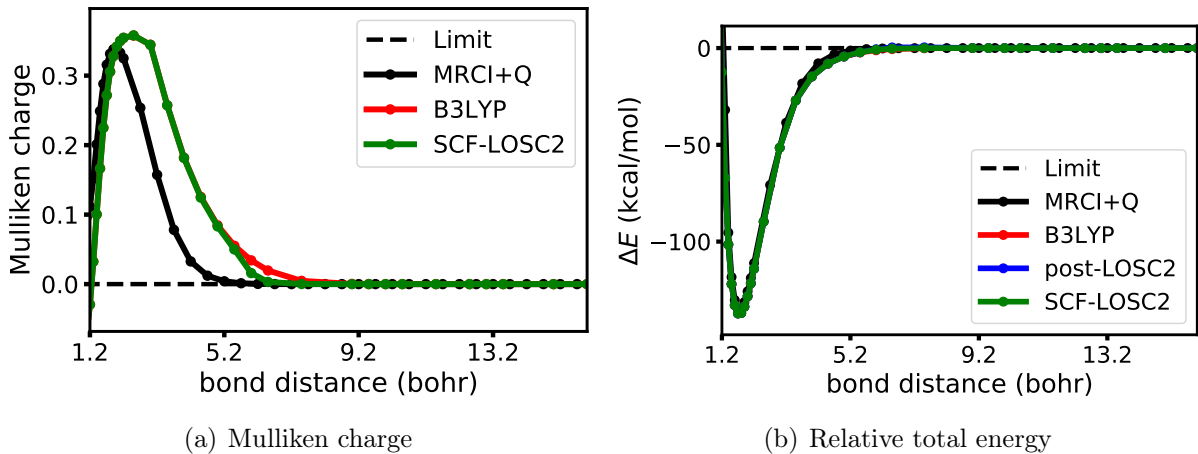


Figure S1: Dissociation of HF molecule: (a) the Mulliken charge of H atom; (b) the relative total energy of HF with respect to H and F atoms.  $\Delta E = E_{\text{HF}} - (E_{\text{H}} + E_{\text{F}})$ . The LOSC2 calculation is associated with B3LYP.

Figure S1 shows the dissociation results for HF molecule. Since  $\text{IP}_{\text{H}} > \text{EA}_{\text{F}}$ , the HF molecule must dissociate into neutral H and F atom. According to Figure S1, we see that B3LYP already describes the electron density quite well for this system. In addition, we see SCF-LOSC-B3LYP preserves the good results for the Mulliken charge, and both SCF-LOSC-B3LYP and post-LOSC-B3LYP preserve the good results for the relative total energy.

Tables S1 – S6 show the detailed data for the relative total energies and Mulliken charges for the HF, LiH and LiF molecules along their dissociations. Tables S7 – S10 show the detailed data for the relative total energies, Mulliken charges, first ionization potentials (IPs) and electron affinities (EAs) for the D-A complex system along its dissociation.

Table S1: Relative total energies (in kcal/mol) of HF molecule to H and F atoms along the dissociation of HF. LOOSC2 calculation is associated with B3LYP. The bond length is in bohr.

bond length	B3LYP	post-LOOSC2	SCF-LOOSC2	MRCI+Q
1.2	-12.4575	-12.4574	-12.4574	30.2242
1.3	-67.1318	-67.1317	-67.1317	-31.9542
1.4	-101.5012	-101.5012	-101.5012	-95.3494
1.5	-121.9666	-121.9666	-121.9666	-118.3303
1.6	-132.8496	-132.8496	-132.8495	-130.1832
1.7	-137.1426	-137.1425	-137.1425	-134.8318
1.8	-136.9154	-136.9153	-136.9153	-134.659
1.9	-133.6136	-133.6134	-133.6134	-131.2544
2.0	-128.2557	-128.2556	-128.2556	-125.7169
2.1	-121.5580	-121.5578	-121.5578	-118.8194
2.2	-114.0342	-114.0340	-114.0340	-111.1109
2.5	-89.6527	-89.6525	-89.6525	-86.4992
3.0	-51.5166	-51.5160	-51.5160	-50.0269
3.5	-27.0746	-27.0738	-27.0738	-25.031
4.0	-14.7166	-14.7122	-14.7122	-11.1439
4.5	-8.0865	-8.0680	-8.0682	-4.6162
5.0	-4.3961	-4.3606	-4.3613	-1.8574
5.5	-2.2891	-2.1663	-2.1750	-0.7509
6.0	-1.1564	-0.6024	-0.8187	-0.3099
6.5	-0.5468	0.3367	-0.2678	-0.1308
7.5	-0.0984	0.3739	-0.0293	-0.0251
9.0	-0.0011	0.0365	0.0032	-0.0021
9.5	-0.0021	0.0111	-0.0006	0.0084
10.0	-0.0227	-0.0185	-0.0223	0.0269
10.5	-0.0167	-0.0154	-0.0165	0.0275
11.5	-0.0031	-0.0031	-0.0031	0.0281
12.5	-0.0304	-0.0304	-0.0304	0.0284
13.0	-0.0206	-0.0206	-0.0206	0.0285
13.5	-0.0082	-0.0082	-0.0082	0.0286
15.0	-0.0175	-0.0175	-0.0175	0.0287
16.0	-0.0184	-0.0184	-0.0184	0.0287

Table S2: Mulliken charges of H atom along the dissociation of HF molecule. LOSC2 calculation is associated with B3LYP. Bond length is in bohr.

bond length	B3LYP	SCF-LOSC2	MRCI+Q
1.2	-0.0294	-0.0293	0.1115
1.3	0.0324	0.0324	0.1518
1.4	0.1004	0.1004	0.2011
1.5	0.1664	0.1664	0.2489
1.6	0.2249	0.2249	0.2882
1.7	0.2718	0.2719	0.3156
1.8	0.3058	0.3058	0.3314
1.9	0.3281	0.3282	0.3379
2.0	0.3418	0.3419	0.3376
2.1	0.3498	0.3499	0.3329
2.2	0.3543	0.3544	0.3250
2.5	0.3577	0.3579	0.2875
3.0	0.3444	0.3444	0.1959
3.5	0.2574	0.2574	0.1058
4.0	0.1819	0.1816	0.0471
4.5	0.1255	0.1245	0.0182
5.0	0.0846	0.0831	0.0064
5.5	0.0551	0.0499	0.0020
6.0	0.0342	0.0159	0.0006
6.5	0.0196	0.0031	0.0001
7.5	0.0047	0.0002	0.0000
9.0	0.0003	0.0000	0.0000
9.5	0.0001	0.0000	0.0000
10.0	0.0000	0.0000	0.0000
10.5	0.0000	0.0000	0.0000
11.5	0.0000	0.0000	0.0000
12.5	0.0000	0.0000	0.0000
13.0	0.0000	0.0000	0.0000
13.5	0.0000	0.0000	0.0000
15.0	0.0000	0.0000	0.0000
16.0	0.0000	0.0000	0.0000

Table S3: Relative total energies (in kcal/mol) of LiH molecule to Li and H atoms along the dissociation of LiH. LOSC2 calculation is associated with B3LYP. Bond length is in bohr.

bond length	B3LYP	post-LOSC2	SCF-LOSC2	MRCI+Q
2.0	-15.4288	-15.3627	-15.3710	-10.7844
2.1	-26.1238	-26.0563	-26.0645	-21.9963
2.2	-34.6988	-34.6291	-34.6374	-30.9907
2.3	-41.4997	-41.4273	-41.4357	-38.1313
2.4	-46.8077	-46.7320	-46.7406	-43.7218
2.5	-50.8853	-50.8059	-50.8147	-48.0160
2.6	-53.9230	-53.8392	-53.8483	-51.2262
2.7	-56.0525	-55.9640	-55.9733	-53.5307
2.8	-57.4136	-57.3198	-57.3295	-55.0788
2.9	-58.1528	-58.0533	-58.0633	-55.9962
3.0	-58.3849	-58.2803	-58.2905	-56.3885
3.1	-58.1958	-58.0851	-58.0957	-56.3445
3.2	-57.6616	-57.5443	-57.5551	-55.9389
3.3	-56.8490	-56.7263	-56.7372	-55.2348
3.4	-55.8076	-55.6754	-55.6868	-54.2853
3.5	-54.5728	-54.4314	-54.4433	-53.1353
3.6	-53.1749	-53.0238	-53.0360	-51.8228
3.7	-51.6449	-51.5349	-51.5416	-50.3799
3.8	-50.0139	-49.8979	-49.9046	-48.8338
3.9	-48.3078	-48.1849	-48.1917	-47.2078
4.0	-46.5455	-46.4138	-46.4207	-45.5215
4.5	-37.3273	-37.1323	-37.1405	-36.6986
5.0	-28.3053	-27.9964	-28.0072	-28.0979
5.5	-20.4636	-20.0047	-20.0122	-20.4109
6.0	-14.7873	-13.7717	-13.7773	-14.0005
6.5	-10.6989	-8.3763	-8.3954	-9.0484
7.0	-7.6789	-4.2302	-4.4422	-5.5486
7.5	-5.4981	-1.6570	-2.2771	-3.2814
8.0	-3.8554	0.5482	-0.9276	-1.9048
8.5	-2.6695	1.6374	-0.5048	-1.0987
9.0	-1.7990	2.3561	-0.2999	-0.6340
9.5	-1.1380	2.7338	-0.1672	-0.3676
10.0	-0.6977	2.7231	-0.1220	-0.2148
10.5	-0.3892	2.3366	-0.0911	-0.1270
11.0	-0.1671	1.2635	-0.0457	-0.0762
11.5	-0.0865	0.1972	-0.0338	-0.0466
12.0	-0.0673	0.0479	-0.0386	-0.0292
12.5	-0.0280	0.0294	-0.0111	-0.0187
13.0	0.0246	0.0550	0.0348	-0.0124
13.5	0.0042	0.0214	0.0106	-0.0085

Table S3 continued: LiH relative total energy.

bond length	B3LYP	post-LOSC2	SCF-LOSC2	MRCI+Q
14.0	-0.0783	-0.0683	-0.0742	-0.0060
14.5	-0.1195	-0.1134	-0.1168	-0.0043
15.0	-0.0888	-0.0851	-0.0870	-0.0032
15.5	-0.0357	-0.0334	-0.0345	-0.0024
16.0	-0.0369	-0.0355	-0.0362	-0.0019

Table S4: Mulliken charges of Li atom along the dissociation of LiH molecule. LOSC2 calculation is associated with B3LYP. Bond length is in bohr.

bond length	B3LYP	SCF-LOSC2	MRCI+Q
2.0	-0.1833	-0.1845	0.0117
2.1	-0.1026	-0.1033	0.0341
2.2	-0.0294	-0.0296	0.0558
2.3	0.0346	0.0347	0.0765
2.4	0.0887	0.0892	0.0958
2.5	0.1332	0.1341	0.1138
2.6	0.1691	0.1705	0.1305
2.7	0.1980	0.1999	0.1461
2.8	0.2214	0.2236	0.1608
2.9	0.2402	0.2429	0.1747
3.0	0.2555	0.2578	0.1878
3.1	0.2679	0.2704	0.1999
3.2	0.2781	0.2812	0.2110
3.3	0.2865	0.2904	0.2211
3.4	0.2936	0.2980	0.2300
3.5	0.2998	0.3045	0.2379
3.6	0.3051	0.3102	0.2447
3.7	0.3098	0.3138	0.2505
3.8	0.3139	0.3180	0.2553
3.9	0.3175	0.3216	0.2592
4.0	0.3205	0.3248	0.2623
4.5	0.3308	0.3365	0.2662
5.0	0.3362	0.3436	0.2539
5.5	0.3018	0.3087	0.2265
6.0	0.2616	0.2679	0.1850
6.5	0.2279	0.2176	0.1350
7.0	0.1974	0.1488	0.0873
7.5	0.1707	0.0844	0.0513
8.0	0.1463	0.0220	0.0283
8.5	0.1243	0.0032	0.0150
9.0	0.1041	-0.0017	0.0078

Table S4 continued: Mulliken charge for LiH.

bond length	B3LYP	SCF-LOSC2	MRCI+Q
9.5	0.0851	-0.0026	0.0039
10.0	0.0666	-0.0024	0.0019
10.5	0.0475	-0.0020	0.0008
11.0	0.0218	-0.0015	0.0003
11.5	0.0026	-0.0012	0.0001
12.0	0.0002	-0.0009	-0.0001
12.5	-0.0003	-0.0007	-0.0001
13.0	-0.0004	-0.0006	-0.0001
13.5	-0.0004	-0.0004	-0.0001
14.0	-0.0003	-0.0003	-0.0001
14.5	-0.0003	-0.0002	-0.0001
15.0	-0.0002	-0.0002	-0.0001
15.5	-0.0001	-0.0001	0.0000
16.0	-0.0001	-0.0001	0.0000

Table S5: Relative total energies (in kcal/mol) of LiF molecule to Li and F atoms along the dissociation of LiF molecule. LOSC2 calculation is associated with B3LYP. Bond length is in bohr.

bond length	B3LYP	post-LOSC2	SCF-LOSC2	MRCI+Q
2.0	-11.1313	-11.1282	-11.1292	7.6169
2.1	-46.2190	-46.2168	-46.2176	-32.2749
2.2	-72.8208	-72.8190	-72.8196	-62.3335
2.3	-93.5515	-93.5499	-93.5505	-84.7549
2.4	-108.7332	-108.7308	-108.7313	-101.2518
2.5	-119.4273	-119.4239	-119.4246	-113.1557
2.6	-127.0197	-127.0153	-127.0161	-121.5001
2.7	-131.9696	-131.9637	-131.9648	-127.0870
2.8	-134.3851	-134.3777	-134.3790	-130.5384
2.9	-135.1401	-135.1308	-135.1324	-132.3373
3.0	-135.0463	-135.0348	-135.0368	-132.8588
3.1	-134.4564	-134.4424	-134.4448	-132.3951
3.2	-133.3654	-133.3486	-133.3515	-131.1742
3.3	-131.7308	-131.7106	-131.7141	-129.3739
3.4	-129.5920	-129.5678	-129.5720	-127.1337
3.5	-127.0081	-126.9795	-126.9845	-124.5628
3.6	-124.0522	-124.0185	-124.0243	-121.7469
3.7	-120.8511	-120.8147	-120.8216	-118.7535
3.8	-117.5881	-117.5464	-117.5546	-115.6353
3.9	-114.3647	-114.3175	-114.3259	-112.4343
4.0	-111.1560	-111.0940	-111.1049	-109.1833
4.5	-94.9697	-94.8466	-94.8694	-92.9192
5.0	-80.2682	-79.9710	-80.0341	-77.6557
5.5	-67.6008	-66.7450	-67.0577	-63.9408
6.0	-56.5122	-54.2887	-55.3087	-51.8360
6.5	-47.7051	-40.8312	-44.7600	-41.1991
7.0	-41.0785	-29.2018	-34.9247	-31.8369
7.5	-36.2685	-20.2362	-26.4268	-23.5722
8.0	-32.2866	-12.8701	-18.3563	-16.2644
8.2	-31.0497	-10.4710	-15.4437	-13.5888
8.4	-29.9576	-8.3157	-12.7038	-11.0493
8.6	-28.9236	-6.3162	-10.0537	-8.6461
8.8	-27.9247	-4.4313	-7.4598	-6.3781
9.0	-26.9809	-2.6735	-4.9560	-4.1863
9.2	-26.1236	-1.1241	-2.6175	-3.1530
9.4	-25.3830	0.3131	-0.4215	-2.4920
9.6	-24.7567	1.5742	0.2256	-2.0419
9.8	-24.1975	2.7152	0.1614	-1.7255
10.0	-23.6657	3.7701	0.1320	-1.4984



Table S5 continued: LiF relative total energy:

bond length	B3LYP	post-LOSC2	SCF-LOSC2	MRCI+Q
10.5	-22.4132	6.1178	0.1767	-1.1606
11.0	-21.3784	7.9844	0.1953	-0.9953
11.5	-20.6328	9.3634	0.1086	-0.9096
12.0	-19.9551	10.5154	0.1066	-0.8630
12.5	-19.2706	11.5527	0.1744	-0.8367
13.0	-18.7236	12.3971	0.1657	-0.8212
13.5	-18.5438	12.8576	-0.0797	-0.8118
14.0	-18.2962	13.4397	-0.1830	-0.8058
14.5	-17.8053	14.0105	-0.0191	-0.8020
15.0	-17.4103	14.7710	0.0037	-0.7995
15.5	-17.0572	15.2449	0.0297	-0.7979
16.0	-16.9598	15.4776	-0.1351	-0.7968

Table S6: Mulliken charges of Li atom along the dissociation of LiF molecule. LOSC2 calculation is associated with B3LYP. Bond length is in bohr.

bond length	B3LYP	SCF-LOSC2	MRCI+Q
2.0	0.1009	0.1016	0.4072
2.1	0.1382	0.1389	0.4185
2.2	0.1698	0.1696	0.4293
2.3	0.1963	0.1970	0.4398
2.4	0.2236	0.2245	0.4502
2.5	0.2528	0.2537	0.4605
2.6	0.2838	0.2848	0.4707
2.7	0.3164	0.3175	0.4807
2.8	0.3503	0.3515	0.4904
2.9	0.3839	0.3852	0.4998
3.0	0.4144	0.4158	0.5089
3.1	0.4419	0.4434	0.5177
3.2	0.4678	0.4696	0.5264
3.3	0.4926	0.4945	0.5349
3.4	0.5148	0.5169	0.5434
3.5	0.5337	0.5361	0.5519
3.6	0.5491	0.5517	0.5604
3.7	0.5611	0.5640	0.5690
3.8	0.5705	0.5736	0.5777
3.9	0.5782	0.5814	0.5863
4.0	0.5850	0.5888	0.5950
4.5	0.6135	0.6195	0.6368
5.0	0.6339	0.6445	0.6745
5.5	0.6470	0.6669	0.7079

Table S6 continued: Mulliken charge for LiF.

bond length	B3LYP	SCF-LOSC2	MRCI+Q
6.0	0.6529	0.6891	0.7386
6.5	0.6150	0.7160	0.7676
7.0	0.5744	0.7417	0.7948
7.5	0.5443	0.7652	0.8192
8.0	0.5192	0.7847	0.8399
8.2	0.5102	0.7858	0.8470
8.4	0.5019	0.7925	0.8532
8.6	0.4939	0.7972	0.8587
8.8	0.4864	0.7999	0.8633
9.0	0.4791	0.7994	0.0738
9.2	0.4722	0.7948	0.0447
9.4	0.4656	0.7527	0.0295
9.6	0.4594	-0.0030	0.0202
9.8	0.4538	-0.0028	0.0141
10.0	0.4484	-0.0025	0.0100
10.5	0.4363	-0.0020	0.0044
11.0	0.4255	-0.0016	0.0020
11.5	0.4164	-0.0012	0.0008
12.0	0.4083	-0.0009	0.0003
12.5	0.4008	-0.0007	0.0001
13.0	0.3939	-0.0005	0.0000
13.5	0.3888	-0.0004	0.0000
14.0	0.3836	-0.0003	0.0000
14.5	0.3786	-0.0002	0.0000
15.0	0.3736	-0.0002	0.0000
15.5	0.3684	-0.0001	0.0000
16.0	0.3652	-0.0001	0.0000

Table S7: Relative total energies (in kcal/mol) of the D-A complex system to the donor and acceptor subsystems along the dissociation of D-A complex system. LOOSC2 calculation is associated with BLYP. The separation distance of D-A complex is in Angstrom. D3BJ is obtained from BLYP and added to all the DFT energy results.

distance	MP2	BLYP	post-LOOSC2	SCF-LOOSC2	BLYP+D3BJ	post-LOOSC2+D3BJ	SCF-LOOSC2+D3BJ
2.0	-10.1188	24.0480	23.9289	23.9311	0.2372	0.1180	0.1202
2.1	-14.7578	15.5839	15.5148	15.5121	-6.7456	-6.8147	-6.8174
2.2	-17.4782	9.4401	9.4186	9.4096	-11.3526	-11.3741	-11.3831
2.3	-18.8295	5.1131	5.1393	5.1237	-14.1209	-14.0947	-14.1103
2.4	-19.2206	2.1510	2.2190	2.2137	-15.5295	-15.4614	-15.4668
2.5	-18.9537	-0.0009	0.1769	0.2277	-16.1564	-15.9785	-15.9277
2.6	-18.2509	-1.5905	-1.3902	-1.1377	-16.2699	-16.0696	-15.8172
2.7	-17.2745	-2.7724	-2.5995	-2.0587	-16.0423	-15.8693	-15.3285
2.8	-16.1424	-3.5927	-3.4372	-2.6196	-15.5334	-15.3779	-14.5603
2.9	-14.9387	-4.1067	-3.9674	-2.8956	-14.8087	-14.6694	-13.5976
3.0	-13.7228	-4.3892	-4.2681	-2.9607	-13.9492	-13.8281	-12.5208
3.1	-12.5350	-4.5160	-4.4099	-2.8787	-13.0334	-12.9273	-11.3961
3.2	-11.4014	-4.5531	-4.4616	-2.7242	-12.1263	-12.0349	-10.2974
3.3	-10.3379	-4.5575	-4.4831	-2.5748	-11.2820	-11.2076	-9.2993
3.4	-9.3527	-4.5545	-4.4926	-2.4502	-10.5204	-10.4585	-8.4161
3.5	-8.4490	-4.5475	-4.4934	-2.3470	-9.8386	-9.7845	-7.6381
3.6	-7.6265	-4.5330	-4.4914	-2.2637	-9.2259	-9.1843	-6.9566
3.7	-6.8824	-4.4994	-4.4672	-2.1627	-8.6636	-8.6314	-6.3269
3.8	-6.2126	-4.4389	-4.4150	-2.0270	-8.1366	-8.1126	-5.7246
3.9	-5.6121	-4.3588	-4.3421	-1.8683	-7.6453	-7.6286	-5.1548
4.0	-5.0751	-4.2737	-4.2628	-1.7105	-7.1981	-7.1871	-4.6349
5.0	-2.0419	-3.9188	-3.9338	-0.9799	-4.9040	-4.9191	-1.9651
6.0	-0.9841	-3.6322	-3.6509	-0.5397	-4.0169	-4.0356	-0.9244
7.0	-0.5361	-3.4487	-3.4669	-0.2977	-3.6184	-3.6367	-0.4675
8.0	-0.3135	-3.3296	-3.3474	-0.1631	-3.4120	-3.4299	-0.2456
9.0	-0.1932	-3.2451	-3.2626	-0.0847	-3.2884	-3.3058	-0.1279
10.0	-0.1242	-3.1816	-3.1988	-0.0376	-3.2058	-3.2229	-0.0617

Table S8: Mulliken charges of the donor molecule along the dissociation of D-A complex system. LOOSC2 calculation is associated with B3LYP. Separation distance is in Angstrom.

distance	MP2	BLYP	SCF-LOOSC2
2.0	0.2060	0.2675	0.2666
2.1	0.1678	0.2336	0.2331
2.2	0.1358	0.2031	0.2025
2.3	0.1097	0.1756	0.1738
2.4	0.0887	0.1773	0.1478
2.5	0.0720	0.1829	0.1246
2.6	0.0586	0.1923	0.1035
2.7	0.0479	0.1993	0.0844
2.8	0.0393	0.2043	0.0675
2.9	0.0323	0.2082	0.0534
3.0	0.0266	0.2115	0.0419
3.1	0.0219	0.2141	0.0326
3.2	0.0181	0.2164	0.0252
3.3	0.0150	0.2185	0.0194
3.4	0.0124	0.2200	0.0152
3.5	0.0102	0.2212	0.0121
3.6	0.0085	0.2222	0.0100
3.7	0.0070	0.2228	0.0083
3.8	0.0058	0.2230	0.0070
3.9	0.0047	0.2231	0.0059
4.0	0.0039	0.2232	0.0050
5.0	0.0003	0.2190	0.0005
6.0	0.0000	0.2128	0.0000
7.0	0.0000	0.2069	0.0000
8.0	0.0000	0.2017	0.0000
9.0	0.0000	0.1971	0.0000
10.0	0.0000	0.1932	0.0000

Table S9: The first ionization potentials (IPs, in eV) of the D-A complex along the its dissociation. The negative energy of the highest occupied molecular orbital from DFT is used to evaluate the IP. The IP of the donor molecule is also listed in the table for comparison. LOSC2 and GW calculation is associated with BLYP. evGW refers to eigenvalue self-consistent GW calculation. Distance is in Angstrom.

distance	$G_0W_0$	evGW	BLYP	post-LOSC2	SCF-LOSC2
2.0	7.1655	7.8547	5.0565	8.2385	8.2359
3.0	6.7645	7.1875	4.9001	8.0881	7.6724
4.0	6.7213	7.1155	4.8926	8.0395	7.4042
5.0	6.7431	7.1306	4.8833	8.0136	7.2949
6.0	6.7608	7.1494	4.8755	7.9978	7.2351
7.0	6.7752	7.1650	4.8695	7.9882	7.1993
8.0	6.7885	7.1734	4.8649	7.9819	7.1762
9.0	6.7996	7.1846	4.8614	7.9775	7.1605
10.0	6.8092	7.1946	4.8586	7.9743	7.1495
Donor	6.5812	7.0720	4.0021	7.1168	7.1153

Table S10: The first electron affinities (EAs, in eV) of D-A complex along its dissociation. The negative energy of the lowest unoccupied molecular orbital from DFT is used to evaluate the EA. The EA of the acceptor molecule is also listed in the table for comparison. LOSC2 and GW calculation is associated with BLYP. evGW refers to the eigenvalue self-consistent calculation. Distance is in Angstrom.

distance	$G_0W_0$	evGW	BLYP	post-LOSC2	SCF-LOSC2
2.0	2.5904	2.2184	4.4780	2.3862	2.3950
3.0	1.7791	1.5800	4.7850	2.7272	3.1431
4.0	1.8738	1.6752	4.7620	2.7066	3.3499
5.0	1.8834	1.6862	4.7539	2.7012	3.4283
6.0	1.8738	1.6748	4.7495	2.6964	3.4680
7.0	1.8610	1.6626	4.7471	2.6937	3.4919
8.0	1.8476	1.6486	4.7456	2.6919	3.5072
9.0	1.8359	1.6337	4.7447	2.6907	3.5174
10.0	1.8255	1.6229	4.7442	2.6899	3.5246
Acceptor	3.3117	2.9932	5.5860	3.5161	3.5304

## 2. Atomization energies, reaction barriers, IPs and EAs

We use the same test sets to investigate the performance of the new SCF-LOSC approach for the atomization energies, reaction barriers, IPs and EAs. See Ref S7 for more information about molecular geometries and reference values for these test sets. Table S11 shows the results from different methods for atomization energies, reaction barriers, IPs and EAs. Detailed data for each test set are summarized in Tables S13 – S20. The negative HOMO/LUMO energies from DFT calculation is used to evaluate the first IP/EA respectively. Table S12 shows the comparison of the negative HOMO energies of polyacetylene from different methods with the first IP. All the DFT calculation are performed from using an in-house developed QM<sup>4</sup>D package.<sup>S1</sup> 6-311++G(3df, 3pd) is used as the basis set for the results shown in Tables S11, S13 – S20. cc-pVDZ is used as the basis set for the results shown in Table S12. aug-cc-pVTZ-RIFIT is the fitting basis used in the construction of curvature matrix in LOSC.

Table S11: Mean absolute errors (MAEs) for atomization energies (AE), reaction barriers (RB), IPs and EAs from different methods. Results of AE and RB test sets is in kcal/mol. Results of IP and EA test sets is in eV.

Test set	DFA			post-LOSC2			SCF-LOSC2		
	LDA	BLYP	B3LYP	LDA	BLYP	B3LYP	LDA	BLYP	B3LYP
<b>AE</b>									
G2-1	42.20	4.94	2.45	42.19	4.93	2.45	42.19	4.93	2.45
NonHydrocarbon	97.74	14.73	7.64	97.74	14.73	7.65	97.74	14.73	7.65
Hydrocarbon	140.95	10.36	3.47	140.94	10.38	3.48	140.94	10.38	3.48
SubHydrocarbon	124.34	6.23	2.52	124.32	6.24	2.53	124.32	6.24	2.52
Radical	78.02	3.89	2.26	78.00	3.91	2.26	78.00	3.91	2.26
<b>RB</b>									
HTBH38	17.36	7.67	4.35	17.17	7.49	4.35	17.21	7.54	4.35
NHTBH38	14.22	10.11	6.38	14.24	10.14	6.38	14.23	10.12	6.38
<b>IP &amp; EA</b>									
IP	4.29	4.50	3.19	0.49	0.62	0.35	0.50	0.62	0.35
EA	3.79	3.41	2.57	0.53	0.50	0.44	0.54	0.51	0.44

Table S12: Negative HOMO energies (in eV) of polyacetylene with different unit numbers calculated from different DFAs and compared with the first IP from RASPT2.

units	RASPT2	DFA			post-LOSC2			SCF-LOSC2		
		LDA	BLYP	B3LYP	LDA	BLYP	B3LYP	LDA	BLYP	B3LYP
1	10.48	6.71	6.34	7.46	10.46	10.11	10.46	10.46	10.11	10.46
2	9.18	5.84	5.46	6.43	9.49	9.12	8.35	9.49	9.12	8.35
3	8.18	5.40	5.01	5.89	8.84	8.47	8.03	8.84	8.47	8.03
4	7.69	5.14	4.74	5.56	8.01	7.66	7.77	8.01	7.66	7.77
5	7.33	4.97	4.56	5.34	7.78	7.41	7.59	7.80	7.42	7.60
6	7.04	4.84	4.43	5.17	7.56	7.19	7.41	7.59	7.21	7.42
7	6.85	4.75	4.33	5.05	7.48	7.10	7.19	7.53	7.15	7.20
8	6.66	4.68	4.25	4.95	7.45	6.95	7.15	7.53	7.03	7.18
9	6.56	4.62	4.19	4.87	7.23	6.85	6.93	7.32	6.94	6.97
10	6.41	4.57	4.14	4.80	7.08	6.61	6.84	7.19	6.72	6.89
MAE		2.49	2.89	2.09	0.50	0.20	0.33	0.54	0.24	0.35

Table S13: Detailed data for the atomization energies (in kcal/mol) of the G2-1 test set. NA means the data is not available because of the SCF convergence issue from DFT.

Molecule	Ref	DFA			post-LOSC2			SCF-LOSC2		
		LDA	BLYP	B3LYP	LDA	BLYP	B3LYP	LDA	BLYP	B3LYP
BeH	49.8	60.26	56.91	57.89	60.24	56.89	57.88	60.24	56.89	57.88
CH	83.9	92.27	85.5	85.43	92.26	85.49	85.43	92.26	85.49	85.43
CH2_3B1	190	NA	183.78	185.02	NA	183.77	185.02	NA	183.77	185.02
CH2_1A1	180.6	201.83	178.97	180.82	201.82	178.97	180.81	201.82	178.97	180.81
CH3	306.6	338.78	306.75	309.79	338.77	306.74	309.78	338.77	306.74	309.78
CH4	419.2	461.87	416.59	420.74	461.86	416.59	420.73	461.86	416.59	420.73
NH	83.5	95.3	89.45	88.02	95.29	89.44	88.02	95.29	89.44	88.02
NH2	181.5	207.72	189.44	187.92	207.71	189.43	187.92	207.71	189.43	187.92
NH3	297.5	337.02	301.6	300.9	337.01	301.58	300.9	337.01	301.59	300.9
OH	106.3	124.28	109.9	108.36	124.28	109.89	108.36	124.28	109.89	108.36
H2O	232.2	266.72	233.04	231.19	266.72	233.04	231.19	266.72	233.04	231.19
HF	140.8	162.58	141.55	139.6	162.58	141.54	139.6	162.58	141.54	139.6
SiH2_1A1	151.4	NA	151.53	153.41	NA	151.53	153.41	NA	151.53	153.41
SiH2_3B1	130.6	NA	130.22	132.93	NA	130.22	132.93	NA	130.22	132.93
SiH3	225.1	NA	223.95	228.23	NA	223.95	228.23	NA	223.95	228.23
SiH4	321.4	NA	317.19	323.32	NA	317.2	323.32	NA	317.2	323.32
PH2	152.8	173.39	157.25	158.46	173.39	157.24	158.45	173.39	157.25	158.45
PH3	241.8	269.19	242.07	244.53	269.19	242.07	244.53	269.19	242.07	244.53
H2S	182.3	206.19	180.63	182.08	206.18	180.62	182.08	206.18	180.62	182.08
HCl	106.4	NA	104.58	105.21	NA	104.58	105.21	NA	104.58	105.21
C2H2	405.3	459.03	404.64	402.5	459.03	404.64	402.5	459.03	404.64	402.5
C2H4	562.6	631.66	560.4	562.96	631.65	560.4	562.96	631.65	560.4	562.96
C2H6	710.7	793.29	703.96	711.3	793.29	703.95	711.3	793.29	703.95	711.3
CN	180.9	217.91	189.16	178.55	217.9	189.15	178.55	217.9	189.15	178.55
HCN	312.5	359.69	319.84	312.28	359.69	319.84	312.27	359.69	319.84	312.27
CO	259.3	298.57	262.13	255.04	298.57	262.13	255.04	298.57	262.13	255.04
HCO	278.7	332.87	287.52	280.58	332.86	287.51	280.58	332.86	287.51	280.58
H2CO	373.7	433.52	378.12	373.65	433.5	378.1	373.64	433.5	378.1	373.64
H3COH	511.9	586.42	511.14	511.93	586.41	511.13	511.92	586.41	511.13	511.92
N2	228.6	264.8	238.7	226.78	264.8	238.7	226.78	264.8	238.7	226.78
H2NNH2	437.8	515.29	447.3	444	515.27	447.28	443.99	515.27	447.28	443.99
NO	152.8	NA	166.26	155.38	NA	166.26	155.38	NA	166.26	155.38
O2	120.5	173.17	135.64	122.31	173.17	135.64	122.31	173.17	135.64	122.31
HOOH	268.7	334.9	276.38	267.15	334.9	276.38	267.15	334.9	276.38	267.15
F2	38.5	76.57	48.23	35.93	76.57	48.23	35.93	76.57	48.23	35.93
CO2	389.2	473.14	400.78	387.96	473.14	400.78	387.96	473.14	400.78	387.96
Si2	74.7	NA	75.92	74.44	NA	75.92	74.44	NA	75.92	74.44
P2	117.3	142.26	121.15	114.82	142.27	121.15	114.82	142.27	121.15	114.82
S2	101.7	134.4	107.06	102.72	134.4	107.06	102.72	134.4	107.06	102.72
Cl2	57.9	NA	57.46	54.88	NA	57.46	54.88	NA	57.46	54.88
SiO	192.3	NA	194.61	186.56	NA	194.58	186.55	NA	194.58	186.55
CS	171.3	201.74	172.26	166.25	201.74	172.26	166.24	201.74	172.26	166.24
SO	125.1	166.28	134.63	125.61	166.28	134.62	125.61	166.28	134.62	125.61
ClO	64.4	NA	74.63	65.75	NA	74.63	65.75	NA	74.63	65.75
ClF	61.4	NA	66.85	60.14	NA	66.85	60.14	NA	66.85	60.14
Si2H6	529.7	NA	519.1	529.87	NA	519.11	529.87	NA	519.1	529.87
CH3Cl	394	NA	389.54	392.73	NA	389.53	392.72	NA	389.53	392.72
H3CSH	473	535.96	467.59	471.78	535.95	467.58	471.77	535.95	467.58	471.77
HOCl	164.4	NA	168.79	162.87	NA	168.79	162.87	NA	168.79	162.87
SO2	258.5	332.58	265.34	248.32	332.58	265.33	248.31	332.58	265.33	248.31

Table S14: Detailed data for the atomization energies (in kcal/mol) of the Hydrocarbon test set. NA means the data is not available because of the SCF convergence issue.

Molecule	Ref	DFA			post-LOSC2			SCF-LOSC2		
		LDA	BLYP	B3LYP	LDA	BLYP	B3LYP	LDA	BLYP	B3LYP
propyne	704.1	800.64	700.95	701.88	800.64	700.94	701.88	800.64	700.94	701.88
allene	702.4	804.06	704.02	704.07	804.05	704.01	704.07	804.05	704.01	704.07
cyclopropene	681.9	784.06	676.58	678.5	784.06	676.57	678.5	784.06	676.57	678.5
propene	859.2	969.6	852.61	858.3	969.59	852.6	858.29	969.59	852.6	858.29
cyclopropane	851.8	967.91	841.9	849.6	967.9	841.89	849.6	967.9	841.89	849.6
propane	1004.6	1127.23	992.43	1003.09	1127.21	992.41	1003.08	1127.21	992.41	1003.08
t13butadiene	1011.3	1149.59	1005.57	1009.2	1149.58	1005.55	1009.19	1149.58	1005.55	1009.19
2-butyne	1002.8	1140.85	995.92	999.96	1140.84	995.91	999.95	1140.84	995.91	999.95
methylenecyclopropane	989.4	1137.32	983.88	989.14	1137.31	983.86	989.13	1137.31	983.86	989.13
bicyclobutane	985.9	1134.3	971.36	978.68	1134.3	971.34	978.67	1134.3	971.34	978.67
cyclobutene	1000.4	1144.08	988.07	994.17	1144.07	988.04	994.16	1144.07	988.05	994.16
cyclobutane	1147	1303.66	1130.26	1141.61	1303.65	1130.24	1141.6	1303.65	1130.24	1141.6
isobutene	1156.6	1307.83	1144.22	1153.27	1307.81	1144.19	1153.25	1307.81	1144.2	1153.25
trans-butane	1298.6	1461.25	1280.95	1294.91	1461.24	1280.92	1294.9	1461.24	1280.92	1294.9
isobutane	1300.4	1462.99	1281.29	1295.42	1462.97	1281.26	1295.41	1462.97	1281.26	1295.41
spiropentane	1282.3	1473.68	1265.88	1276.64	1473.66	1265.84	1276.62	1473.67	1265.84	1276.62
benzene	1366.2	1571.99	1356.06	1360.8	1571.98	1356.03	1360.79	1571.98	1356.04	1360.79



Table S15: Detailed data for the atomization energies (in kcal/mol) of the SubHydrocarbon test set. NA means the data is not available because of the SCF convergence issue.

Molecule	Ref	DFA			post-LOSC2			SCF-LOSC2		
		LDA	BLYP	B3LYP	LDA	BLYP	B3LYP	LDA	BLYP	B3LYP
CH2F2	436.3	517.68	438.77	435.74	517.68	438.77	435.74	517.68	438.77	435.74
CHF3	457.8	560.52	460.62	454.71	560.51	460.61	454.7	560.51	460.61	454.7
CH2Cl2	369.6	NA	362.63	364.34	NA	362.62	364.34	NA	362.62	364.34
CHCl3	343.3	NA	333	333.01	NA	332.98	332.99	NA	332.98	332.99
methylamine	581.2	660.53	581.89	584.16	660.51	581.86	584.15	660.52	581.87	584.15
methylcyanide	615.1	704.62	619.59	615.22	704.61	619.58	615.22	704.61	619.58	615.22
nitromethane	600.6	742.94	618.45	602.23	742.92	618.42	602.22	742.92	618.42	602.22
methylnitrite	598.3	736.06	615.75	598.96	736.06	615.74	598.95	736.06	615.74	598.95
methylsilane	626.1	NA	615.85	625.11	NA	615.84	625.11	NA	615.84	625.11
HCOOH	500.7	598.11	507.3	499.36	598.09	507.29	499.36	598.09	507.29	499.36
methylformate	784.2	922.12	788.3	783.14	922.1	788.27	783.13	922.1	788.28	783.13
acetamide	867.2	1010.81	870.82	868.13	1010.76	870.75	868.11	1010.76	870.76	868.11
aziridine	719	831.28	717.99	719.83	831.27	717.98	719.83	831.27	717.98	719.83
cyanogen	502.3	598.35	520.01	501.09	598.32	519.99	501.08	598.32	519.99	501.08
dimethylamine	868.8	988.9	865.15	870.47	988.86	865.1	870.45	988.86	865.1	870.45
trans-ethylamine	875.8	996.55	872.32	877.81	996.5	872.27	877.79	996.5	872.28	877.79
ketene	532.1	627.07	540.55	533.75	627.06	540.55	533.75	627.06	540.55	533.75
oxirane	650	756.88	648.75	648.32	756.86	648.73	648.31	756.86	648.73	648.31
acetaldehyde	676.3	778.37	676.98	675.56	778.33	676.93	675.55	778.34	676.93	675.55
glyoxal	633.4	752.69	641.57	631.06	752.65	641.53	631.04	752.66	641.53	631.04
ethanol	808.8	923.7	802.91	806.96	923.69	802.88	806.95	923.69	802.88	806.96
dimethylether	796.8	911.72	792.81	796.34	911.69	792.76	796.32	911.69	792.76	796.32
thiooxirane	622.9	719.35	615.96	619.76	719.34	615.95	619.76	719.34	615.95	619.76
dimethylsulfoxide	854.2	991.25	846.46	847.6	991.23	846.37	847.57	991.23	846.38	847.57
ethanethiol	767.6	870.42	756.53	763.99	870.4	756.51	763.98	870.4	756.51	763.98
dimethylsulfide	765.9	868.92	756.28	763.29	868.9	756.25	763.27	868.9	756.25	763.27

Table S15 continued.

Molecule	Ref	DFA			post-LOSC2			SCF-LOSC2		
		LDA	BLYP	B3LYP	LDA	BLYP	B3LYP	LDA	BLYP	B3LYP
vinylfluoride	571.5	663.6	573.93	572.36	663.6	573.92	572.36	663.6	573.92	572.36
ethylchloride	690.2	NA	680.49	686.92	NA	680.47	686.91	NA	680.47	686.91
vinylchloride	538.6	NA	538.4	539.49	NA	538.38	539.48	NA	538.38	539.48
acrylonitrile	763.4	878.54	767.37	760.68	878.53	767.35	760.68	878.53	767.35	760.68
acetone	977.1	1120.46	972.66	974.72	1120.42	972.6	974.69	1120.43	972.61	974.7
aceticacid	802.2	940.12	803.33	799.06	940.11	803.3	799.05	940.11	803.31	799.06
acetylfluoride	705.5	829.62	708.26	703.15	829.61	708.24	703.14	829.61	708.24	703.14
acetylchloride	666.9	NA	667.11	663.45	NA	667.09	663.44	NA	667.09	663.44
propylchloride	983.8	NA	968.91	978.67	NA	968.88	978.66	NA	968.88	978.66
isopropanol	1106.3	1261.88	1094.3	1101.77	1261.85	1094.25	1101.75	1261.85	1094.25	1101.75
methylethylether	1093.1	1248.96	1084.52	1091.35	1248.93	1084.46	1091.33	1248.93	1084.47	1091.33
trimethylamine	1158.6	1320.49	1149.84	1158.34	1320.41	1149.73	1158.31	1320.42	1149.74	1158.31
furan	993.1	1164.92	989.89	988.09	1164.91	989.88	988.09	1164.91	989.88	988.09
thiophene	962	1120.36	951.95	953.66	1120.36	951.94	953.66	1120.36	951.94	953.66
pyrrole	1070.5	1249.31	1068.37	1069.01	1249.3	1068.36	1069	1249.3	1068.36	1069
pyridine	1236.3	1439.59	1236.22	1235.34	1439.57	1236.18	1235.32	1439.57	1236.18	1235.32

Table S16: Detailed data for the atomization energies (in kcal/mol) of the Radical test set. NA means the data is not available because of the SCF convergence issue.

Molecule	Ref	DFA			post-LOSC2			SCF-LOSC2		
		LDA	BLYP	B3LYP	LDA	BLYP	B3LYP	LDA	BLYP	B3LYP
H2	109.2	112.79	109.26	110.13	112.79	109.26	110.13	112.79	109.26	110.13
SH	86.7	NA	NA	88.18	NA	NA	88.18	NA	NA	88.18
CCH	265.8	307.92	264.89	262.04	307.92	264.89	262.04	307.92	264.89	262.04
C2H3	443.9	506.54	446.06	446.95	506.53	446.04	446.94	506.53	446.04	446.94
CH3CO	580.9	676.85	NA	582.54	676.82	NA	582.53	676.83	NA	582.53
H2COH	408.9	477.29	NA	411.13	477.28	NA	411.13	477.28	NA	411.13
CH3O	400.5	464.05	NA	403.88	464.03	NA	403.88	464.03	NA	403.88
CH3CH2O	697.1	800	NA	698.21	799.98	NA	698.2	799.98	NA	698.2
CH3S	380.5	435.3	379.55	382.26	435.29	379.54	382.25	435.29	379.54	382.25
C2H5	602.3	676.5	599.21	604.95	676.49	599.19	604.94	676.49	599.19	604.94
CH3_2CH	898.8	1015.01	891.75	900.43	1014.98	891.71	900.41	1014.98	891.71	900.42
CH3_3C	1197	1353.97	1183.96	1195.76	1353.91	1183.87	1195.72	1353.91	1183.88	1195.73
NO2	227.5	322.38	NA	231.99	322.38	NA	231.99	322.38	NA	231.99

Table S17: Detailed data for the reaction barriers (in kcal/mol) of the HTBH38 test set. NA means the data is not available because of the SCF convergence issue.

case	Ref	DFA			post-LOSC2			SCF-LOSC2		
		LDA	BLYP	B3LYP	LDA	BLYP	B3LYP	LDA	BLYP	B3LYP
Forward: $E_{\text{TS}} - \sum E_{\text{reactant}}$										
TS1	5.7	-3.31	-2.5	-0.81	-3.31	-2.5	-0.8	-3.31	-2.5	-0.8
TS2	4.9	-18.38	-3.49	0.52	-18.38	-3.49	0.52	-18.38	-3.49	0.52
TS3	12.1	-5.39	7.1	8.7	-5.38	7.11	8.7	-5.38	7.11	8.7
TS4	6.5	-17.13	-2.71	1.98	-17.12	-2.71	1.98	-17.12	-2.71	1.98
TS5	9.6	-2.88	2.86	4.22	-2.88	2.86	4.22	-2.88	2.86	4.22
TS6	3	-23.82	-9.17	-2.58	-23.67	-9.11	-2.58	-23.69	-9.11	-2.58
TS7	1.7	-13.56	-3.45	-1.51	-13.56	-3.45	-1.51	-13.56	-3.45	-1.51
TS8	3.2	-20.86	-6.06	-0.98	-20.85	-6.05	-0.98	-20.85	-6.05	-0.98
TS9	1.42	-23.99	-11.46	-5.86	-23.99	-11.46	-5.86	-23.99	-11.46	-5.86
TS10	13.47	-10.33	1.66	7.02	-10.31	1.67	7.02	-10.31	1.67	7.02
TS11	3.1	-7.42	-2.56	-1.03	-7.41	-2.55	-1.03	-7.41	-2.55	-1.03
TS12	10.5	-1.95	1.49	4.05	-1.95	1.49	4.05	-1.95	1.49	4.05
TS13	3.5	-6.83	-2.17	-0.55	-6.83	-2.17	-0.54	-6.83	-2.17	-0.54
TS14	9.57	-22.86	-8.65	1.1	-17.15	-5.58	1.11	-18.2	-6.4	1.11
TS15	8	-8.4	3.48	6.07	-8.38	3.5	6.08	-8.38	3.5	6.08
TS16	7.5	-5.81	5.84	8.14	-5.79	5.86	8.14	-5.79	5.86	8.14
TS17	10.4	-9.68	5.21	8.71	-9.62	5.25	8.72	-9.62	5.25	8.72
TS18	14.5	-6.15	7.94	11.25	-6.1	7.98	11.25	-6.11	7.98	11.25
TS19	38.4	24.89	35.71	38.69	24.88	35.7	38.69	24.88	35.7	38.69
Backward: $E_{\text{TS}} - \sum E_{\text{product}}$										
TS1	7.86	NA	2.26	4.14	NA	2.26	4.14	NA	2.26	4.14
TS2	21.2	11.09	10.26	13.25	11.09	10.26	13.25	11.09	10.26	13.25
TS3	15.3	4.76	7.6	9.49	4.77	7.61	9.49	4.77	7.61	9.49
TS4	19.6	2.19	10.54	13.91	2.2	10.54	13.91	2.2	10.54	13.91
TS5	9.6	-2.88	2.86	4.22	-2.88	2.86	4.22	-2.88	2.86	4.22
TS6	12.7	-10.71	1.76	7.29	-10.57	1.83	7.29	-10.58	1.82	7.29
TS7	7.06	NA	1.82	4.23	NA	1.82	4.23	NA	1.82	4.23
TS8	19.9	4.78	12.27	15.57	4.78	12.27	15.57	4.78	12.27	15.57
TS9	33.4	25.51	20.58	23.66	25.51	20.59	23.66	25.51	20.59	23.66
TS10	7.9	-9.23	1.63	4.43	-9.21	1.64	4.44	-9.21	1.64	4.43
TS11	23.2	9.59	21.86	23	9.6	21.87	23.01	9.6	21.87	23.01
TS12	12.87	-13.19	1.01	5.84	-13.19	1.01	5.84	-13.19	1.01	5.84
TS13	16.76	NA	14.16	15.69	NA	14.17	15.69	NA	14.17	15.69
TS14	9.36	NA	-3.41	4.25	NA	-0.34	4.27	NA	-1.15	4.27
TS15	22.4	2.26	13.33	17.11	2.29	13.35	17.12	2.29	13.35	17.12
TS16	18.3	-1.46	10.61	14.57	-1.42	10.64	14.58	-1.42	10.63	14.57
TS17	17.4	2.86	12.61	15.39	2.91	12.64	15.39	2.9	12.63	15.39
TS18	17.8	0.06	10.25	13.32	0.11	10.29	13.32	0.11	10.28	13.32
TS19	38.4	24.89	35.71	38.69	24.88	35.7	38.69	24.88	35.7	38.69

Table S18: Detailed data for the reaction barriers (in kcal/mol) of the NHTBH38 test set. NA means the data is not available because of the SCF convergence issue.

case	Ref	DFA			post-LOSC2			SCF-LOSC2		
		LDA	BLYP	B3LYP	LDA	BLYP	B3LYP	LDA	BLYP	B3LYP
Forward: $E_{\text{TS}} - \sum E_{\text{reactant}}$										
TS1	17.13	2.47	8.51	11.34	2.48	8.51	11.34	2.48	8.51	11.34
TS2	42.18	18.24	25.97	30.96	18.24	25.96	30.96	18.24	25.96	30.96
TS3	18	2.18	9.86	12.47	2.18	9.86	12.47	2.18	9.86	12.47
TS4	30.38	13.2	16.08	21.75	13.21	16.08	21.75	13.21	16.08	21.75
TS5	2.27	-15.83	-11.46	-7.31	-15.83	-11.46	-7.31	-15.83	-11.46	-7.31
TS6	6.75	-11.09	-6.66	-1.21	-10.81	-6.36	-1.18	-10.81	-6.36	-1.18
TS7	-0.34	-12.05	-7.85	-3.86	-12.01	-7.78	-3.83	-12.02	-7.8	-3.84
TS7	13.38	6.53	6.47	10.2	6.07	5.84	10.1	6.23	6.09	10.13
TS9	3.1	-6.49	-3.78	-0.43	-6.44	-3.71	-0.4	-6.45	-3.72	-0.4
TS9	13.41	6.71	5.68	9.17	6.56	5.5	9.12	6.58	5.52	9.13
TS11	-12.54	-23.31	-19.33	-16.5	-23.11	-19.1	-16.44	-23.14	-19.14	-16.45
TS11	3.44	-1.08	-1.73	0.25	-1.44	-2.2	0.14	-1.34	-2.03	0.18
TS13	-2.44	-14.3	-9.75	-5.8	-14.17	-9.52	-5.73	-14.19	-9.57	-5.74
TS13	10.96	47.54	40.19	45.42	47.48	40.13	45.43	47.51	40.18	45.43
TS15	14.36	-2.39	5.21	7.44	-2.38	5.21	7.44	-2.38	5.21	7.44
TS16	3.17	-7.72	-1.96	-0.6	-7.71	-1.96	-0.6	-7.71	-1.96	-0.6
TS17	1.72	-5.52	-0.71	-0.2	-5.52	-0.71	-0.2	-5.52	-0.71	-0.2
TS18	6.85	-5.85	4.65	5.93	-5.84	4.66	5.94	-5.84	4.66	5.94
TS19	48.07	44.71	46.66	47.29	44.71	46.66	47.29	44.71	46.66	47.29
Forward: $E_{\text{TS}} - \sum E_{\text{reactant}}$										
TS1	82.27	32.24	61.75	72.9	32.24	61.75	72.9	32.24	61.75	72.9
TS2	42.18	18.24	25.97	30.96	18.24	25.96	30.96	18.24	25.96	30.96
TS3	18	2.18	9.86	12.47	2.18	9.86	12.47	2.18	9.86	12.47
TS4	57.02	31.71	42.21	48.6	31.71	42.21	48.6	31.71	42.21	48.6
TS5	105.8	69.47	82.09	96.12	69.47	82.09	96.12	69.47	82.09	96.12
TS6	59.16	NA	42.23	51.42	NA	42.53	51.44	NA	42.53	51.44
TS7	-0.34	-12.05	-7.85	-3.86	-12.01	-7.78	-3.83	-12.02	-7.8	-3.84
TS7	13.38	6.53	6.47	10.2	6.07	5.84	10.1	6.23	6.09	10.13
TS9	3.1	-6.49	-3.78	-0.43	-6.44	-3.71	-0.4	-6.45	-3.72	-0.4
TS9	13.41	6.71	5.68	9.17	6.56	5.5	9.12	6.58	5.52	9.13
TS11	20.11	10.39	13.3	18.48	10.58	13.52	18.54	10.56	13.48	18.53
TS11	29.42	21.67	21.08	26.64	21.69	21.09	26.63	21.69	21.09	26.63
TS13	17.66	5.89	9.14	14.21	6.02	9.38	14.28	5.99	9.33	14.27
TS13	47.2	3.33	3.66	7.63	2.79	2.95	7.5	2.97	3.22	7.54
TS15	10.61	9.34	8.41	10.8	9.33	8.4	10.8	9.33	8.4	10.8
TS16	22.68	26.13	23.15	24.45	26.13	23.15	24.44	26.13	23.15	24.44
TS17	41.75	39.31	38.15	41.77	39.3	38.15	41.77	39.3	38.15	41.77
TS18	32.97	33.17	24.97	29.51	33.15	24.94	29.5	33.15	24.95	29.5
TS19	32.82	30.58	31.68	33.32	30.58	31.67	33.32	30.58	31.67	33.32

Table S19: Detailed data for the ionization potentials (in eV) of the IP test set. NA means the data is not available because of the SCF convergence issue.

Molecule	Ref	DFA			post-LOSC2			SCF-LOSC2		
		LDA	BLYP	B3LYP	LDA	BLYP	B3LYP	LDA	BLYP	B3LYP
H4C	14.4	9.45	9.37	10.75	13.82	13.75	14.26	13.81	13.74	14.25
H3N	11.03	6.33	6.17	7.56	11.54	11.4	11.75	11.54	11.39	11.75
HO	13.07	7.4	7.35	8.99	13.55	13.54	13.96	13.55	13.53	13.95
H2O	12.74	7.37	7.18	8.81	13.4	13.24	13.67	13.4	13.23	13.67
HF	16.2	9.78	9.59	11.51	16.98	16.8	17.3	16.97	16.79	17.3
H4Si	12.84	8.51	8.43	9.65	12.02	11.99	12.51	12.01	11.97	12.51
HP	10.18	6.15	5.89	7.02	9.59	9.33	9.78	9.59	9.33	9.78
H2P	9.82	5.98	5.78	6.89	9.4	9.21	9.63	9.4	9.21	9.63
H3P	10.61	6.77	6.59	7.67	10.22	10.06	10.46	10.22	10.06	10.45
HS	10.41	NA	6.09	7.25	NA	9.87	10.28	NA	9.87	10.27
H2S(2B1)	10.48	6.39	6.15	7.31	10.15	9.91	10.33	10.14	9.91	10.32
HCl	12.82	8.14	7.9	9.22	12.4	12.16	12.64	12.4	12.16	12.64
H2C2	11.51	7.37	7.04	8.19	11.32	10.98	11.34	11.32	10.98	11.34
H4C2	10.74	6.96	6.61	7.66	10.67	10.31	10.62	10.66	10.31	10.62
CO	14.08	9.15	9.03	10.56	14.06	13.95	14.52	14.06	13.95	14.52
N2(2Sg)	15.61	10.42	10.26	11.97	14.66	14.51	15.38	14.66	14.51	15.38
O2	12.49	7.02	6.88	8.8	11.65	11.5	12.52	11.65	11.5	12.52
P2	10.82	7.23	6.88	7.82	10.02	9.68	10.05	10.01	9.66	10.05
S2	9.56	5.93	5.72	6.91	8.59	8.37	9.04	8.59	8.37	9.04
Cl2	11.77	7.54	7.29	8.59	10.38	10.12	10.87	10.38	10.12	10.86
FCl	12.95	8.1	7.86	9.34	11.76	11.53	12.34	11.75	11.53	12.34
CS	11.51	7.49	7.34	8.71	11.84	11.69	12.17	11.83	11.69	12.16
BF3	16.18	10.33	10.03	11.97	16.77	16.52	17.09	16.77	16.52	17.09
BCl3	11.91	7.87	7.57	8.88	11.92	11.64	12.11	11.91	11.64	12.1
CO2	13.9	9.33	8.99	10.46	12.9	12.56	13.31	12.9	12.56	13.31
CF2	12.4	7.48	7.35	8.82	11.74	11.59	12.26	11.73	11.59	12.26
COS	11.36	7.64	7.32	8.45	10.74	10.42	10.93	10.74	10.42	10.93
CS2	10.18	6.94	6.62	7.62	9.25	8.93	9.46	9.25	8.93	9.46
H2C	10.4	5.76	5.49	6.81	10.28	10.03	10.45	10.28	10.03	10.45
H3C	9.78	5.4	5.21	6.47	9.8	9.65	10.02	9.79	9.65	10.02
H5C2	8.6	4.55	4.43	5.66	8.46	8.41	8.82	8.45	8.41	8.81
CN	14.22	9.54	9.25	10.53	14.04	13.75	14.13	14.03	13.74	14.13
HCO	9.37	4.96	4.94	6.32	8.57	8.54	9.21	8.57	8.54	9.21
CH2OH	8.18	3.97	3.85	5.18	7.72	7.63	8.22	7.72	7.62	8.22
CH3O	10.94	6.04	6.03	7.59	10.88	10.94	11.37	10.87	10.93	11.37
H4CO	11.17	6.41	6.26	7.76	11.03	11.01	11.44	11.03	11.01	11.43
H3CF	13.47	8.17	8.04	9.66	12.3	12.34	12.79	12.29	12.34	12.78
H2CS	9.47	5.62	5.4	6.54	9.04	8.86	9.3	9.04	8.85	9.3
CH2SH	7.79	4.19	4.03	5.2	7.32	7.17	7.63	7.32	7.16	7.63

Table S19 continued.

Molecule	Ref	DFA			post-LOSC2			SCF-LOSC2		
		LDA	BLYP	B3LYP	LDA	BLYP	B3LYP	LDA	BLYP	B3LYP
H3CCl	11.49	7.19	6.97	8.26	11.04	10.87	11.37	11.04	10.86	11.36
H6C2O	10.89	6.32	6.17	7.65	10.85	10.86	11.25	10.84	10.84	11.25
H4C2O	10.38	6.09	5.92	7.35	10.39	10.3	10.73	10.38	10.28	10.73
H3COF	11.68	6.76	6.62	8.32	10.98	10.92	11.64	10.97	10.91	11.63
H4C2S	9.15	5.47	5.23	6.37	8.97	8.75	9.18	8.96	8.74	9.18
C2N2	13.59	9.55	9.15	10.34	13.86	13.45	13.78	13.86	13.45	13.78
H4B2	10.17	6.47	6.22	7.29	10.1	9.86	10.18	10.09	9.85	10.18
HN	13.48	7.97	7.73	9.36	13.59	13.37	13.89	13.59	13.36	13.89
H2N	12.12	7.26	7.22	8.61	12.54	12.53	12.85	12.53	12.53	12.85
H2N2	10.28	5.71	5.64	7.03	9.32	9.25	9.92	9.32	9.24	9.92
H3N2	8.34	4.16	4.07	5.51	7.98	7.9	8.55	7.98	7.89	8.55
HOF	13.03	7.48	7.31	9.14	12.2	12.04	12.96	12.2	12.04	12.96
H2Si	9.55	5.9	5.76	6.73	8.91	8.77	9.15	8.91	8.77	9.15
H3Si	8.86	5.3	5.12	6.14	8.47	8.34	8.71	8.47	8.34	8.71
H2Si2	8.22	5.21	4.92	5.8	7.66	7.38	7.76	7.65	7.38	7.76
H4Si2	8.36	5.53	5.24	6.01	8.59	8.3	7.97	8.58	8.3	7.97
H5Si2	8.37	5.21	5.01	5.99	8.23	8.07	8.41	8.22	8.07	8.41
H6Si2	10.73	7.36	7.16	8.21	10.15	9.99	10.49	10.14	9.99	10.49
B2F4	13.3	8.63	8.39	9.93	11.74	11.64	12.47	11.72	11.62	12.46
H4C3(cyclo)	10.04	6.23	5.98	7.04	9.2	9.01	9.48	9.2	9.01	9.48
H4C3(allene)	10.31	6.72	6.42	7.51	10.16	9.89	10.28	10.16	9.89	10.27
H7C3	7.8	4.02	3.94	5.14	7.65	7.66	8.07	7.64	7.65	8.06
H4CS	9.55	5.7	5.48	6.63	9.23	9.04	9.47	9.23	9.04	9.47
H4C4O	9.09	5.9	5.53	6.51	8.61	8.26	8.66	8.61	8.25	8.66
H5C4N	8.42	5.37	5.01	5.96	8.23	7.88	8.2	8.23	7.88	8.19

Table S20: Detailed data for the electron affinities (in eV) of the EA test set. NA means the data is not available because of the SCF convergence issue.

Molecule	Ref	DFA			post-LOSC2			SCF-LOSC2		
		LDA	BLYP	B3LYP	LDA	BLYP	B3LYP	LDA	BLYP	B3LYP
HC	1.19	5.78	5.16	4.15	1.16	0.66	0.73	1.16	0.66	0.73
H2C	0.83	3.9	3.6	2.69	-0.35	-0.59	-0.46	-0.36	-0.59	-0.46
H3C	-0.06	3.59	3.06	2.2	-0.45	-0.84	-0.72	-0.45	-0.84	-0.73
HN	0.33	4.86	4.5	3.3	-0.14	-0.41	-0.34	-0.14	-0.41	-0.34
H2N	0.75	5.22	4.62	3.45	0.23	-0.23	-0.17	0.23	-0.24	-0.18
HO	1.83	7.24	6.53	5.03	1.14	0.59	0.55	1.14	0.58	0.55
HSi	1.26	4.44	NA	3.44	1.47	NA	1.16	1.46	NA	1.15
H2Si	1.07	4.25	3.91	3.34	1.27	0.96	1.03	1.27	0.96	1.03
H3Si	0.93	3.98	3.59	3.01	0.94	0.57	0.63	0.93	0.56	0.62
HP	1.02	4.41	4.08	3.39	1.14	0.85	0.89	1.13	0.84	0.89
H2P	1.26	4.67	4.23	3.55	1.37	0.97	1.01	1.37	0.97	1.01
HS	2.36	NA	5.8	4.97	NA	2.07	2.07	NA	2.07	2.06
O2	-0.02	4.96	4.59	3.53	0.51	0.16	0.09	0.51	0.16	0.09
NO	-0.35	NA	4.24	3.27	NA	-0.05	-0.07	NA	-0.06	-0.07
CN	3.93	8.11	7.76	7	3.77	3.52	3.71	3.77	3.52	3.71
OP	1.09	NA	4.33	3.73	NA	1.36	1.4	NA	1.36	1.4
S2	1.64	4.88	4.52	3.97	2.26	1.92	1.91	2.26	1.91	1.91
Cl2	1.16	4.9	4.57	3.89	1.96	1.66	1.59	1.96	1.65	1.59
C2	3.24	NA	7.1	6.24	NA	3.43	3.36	NA	3.43	3.36
C2O	2.18	6.1	5.66	4.87	2.89	2.47	2.36	2.89	2.47	2.36
CF2	-0.28	4.06	3.68	2.85	0.01	-0.36	-0.33	0	-0.37	-0.33
CNO	3.55	7.81	7.2	6.32	4.31	3.75	3.63	4.31	3.75	3.63
NO2	1.53	5.56	5.18	4.46	2.04	1.7	1.7	2.04	1.7	1.7
O3	1.82	6.4	6.08	5.08	2.9	2.59	1.88	2.9	2.59	1.88
OF	1.94	7.18	6.6	5.41	1.98	1.4	1.26	1.98	1.4	1.26
O2S	1.06	4.88	4.57	4.03	2.02	1.72	1.75	2.02	1.72	1.75
OS2	1.88	5.14	4.83	4.43	2.63	2.32	2.5	2.63	2.32	2.49
HC2	2.95	6.89	6.5	5.61	2.06	1.8	2.19	2.05	1.78	2.19
H3C2	0.19	3.69	3.27	2.43	-0.18	-0.57	-0.52	-0.18	-0.58	-0.52
H2C3	1.7	5.35	4.89	4.24	2.55	2.11	2.05	2.54	2.11	2.05
H3C3	0.68	4.1	3.57	2.86	1.3	0.79	0.7	1.3	0.79	0.69
H5C3	0.38	3.73	3.2	2.46	1.05	0.55	0.39	1.04	0.54	0.39
HCO	-0.07	3.65	3.35	2.57	0.09	-0.16	-0.15	0.09	-0.16	-0.15
HCF	0.24	4.54	3.98	3.06	0.38	-0.14	-0.12	0.37	-0.14	-0.12
CH3O	1.43	5.84	5.32	4.12	1.07	0.48	0.34	1.06	0.47	0.34
H3CS	1.88	3.06	2.6	1.89	-0.14	-0.6	-0.57	-0.15	-0.6	-0.58
H2CS	0.31	3.84	3.5	2.88	0.93	0.61	0.61	0.93	0.6	0.61
CH2CN	1.54	5.23	4.68	3.92	2.14	1.63	1.56	2.14	1.63	1.56
CH2NC	0.99	4.68	4.11	3.31	1.57	1.03	0.93	1.57	1.03	0.93



Table S20 continued.

Molecule	Ref	DFA			post-LOSC2			SCF-LOSC2		
		LDA	BLYP	B3LYP	LDA	BLYP	B3LYP	LDA	BLYP	B3LYP
HC2O	2.28	6.13	5.58	4.81	2.93	2.42	2.33	2.93	2.42	2.33
CH2CHO	1.71	5.47	4.92	4.08	2.35	1.86	1.7	2.34	1.85	1.7
CH3CO	0.16	3.27	2.95	2.2	-0.18	-0.43	-0.4	-0.19	-0.44	-0.4
H5C2O	1.57	5.75	5.2	4.05	1.03	0.41	0.32	1.02	0.4	0.31
H5C2S	1.95	5.39	4.96	4.19	1.87	1.43	1.43	1.87	1.42	1.43
HLi	0.31	1.54	1.72	1.41	-0.74	-0.62	-0.42	-0.75	-0.63	-0.43
HNO	-0.07	4.71	4.27	3.27	0.53	0.13	0.06	0.53	0.13	0.06
HO2	0.62	5.31	4.82	3.71	0.72	0.24	0.1	0.72	0.24	0.1

## II. macro-SCF-LOSC

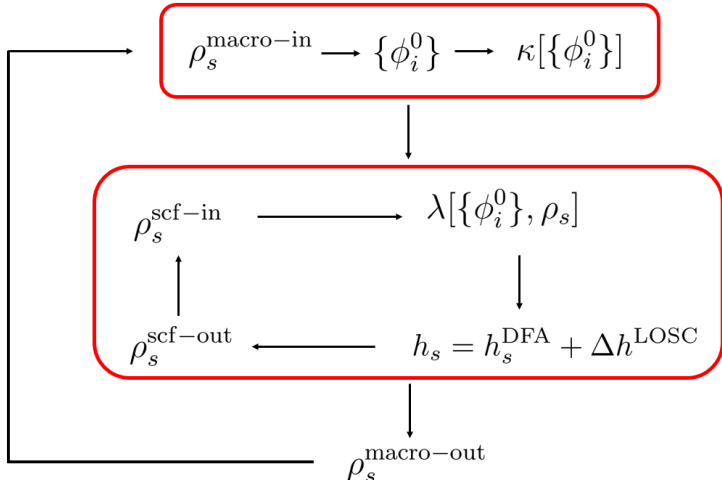


Figure S2: The macro-SCF procedure for LOSC.

The working flow of the macro-SCF-LOSC is shown in Figure S2. The macro-SCF-LOSC includes two layers of SCF cycle. The outer layer SCF cycle is to update the LOs. The inner layer SCF cycle is to update the electron density with the given LOs. The inner layer SCF cycle shares the same spirit of the new SCF-LOSC approach. In details, the macro-SCF-LOSC involves the following steps: (1) start the macro-SCF-LOSC with an initial density guess  $\rho_s^{\text{macro-in}}$ ; (2) apply LOSC localization procedure to produce LOs  $\{\phi_i^0\}$  based on  $\rho_s^{\text{macro-in}}$ ; (3) construct LOSC curvature matrix from  $\{\phi_i^0\}$ ; (4) achieve the convergence of the inner SCF-LOSC calculation with the given  $\{\phi_i^0\}$  and  $\kappa[\{\phi_i^0\}]$  and obtain the converged density as  $\rho_s^{\text{macro-out}}$ ; (5) check the convergence of the macro-SCF-LOSC; go back to step (2) if it is not converged.

Table S21: Total energies (in a.u.) comparison between SCF-LOSC2 and macro-SCF-LOSC2. LOSC2 calculation is associated with B3LYP functional. LiH and LiF molecules are stretched at 14 bohr, and HF molecule is stretched at 16 bohr.

Molecule	SCF-LOSC2	macro-SCF-LOSC2	$\Delta E^1$
HF	-100.2655352	-100.2655352	-1.01E-12
LiH	-7.994964751	-7.994964802	-5.06E-08
LiF	-107.2563249	-107.2565187	-1.94E-04

<sup>1</sup> The energy difference between SCF-LOSC2 and macro-SCF-LOSC2.

To compare the performance between new SCF-LOSC (shown in Figure 2 of the main text) and the macro-SCF-LOSC, Table S21 and S22 show the total energies and Mulliken charges from these two methods for stretched HF, LiH and LiF molecules at large distance. In the cases of stretched HF and LiH, in which the parent functional B3LYP already describes the electron density well, the results from SCF-LOSC and macro-SCF-LOSC are almost the

Table S22: Mulliken charge (in a.u.) comparison between SCF-LOSC2 and macro-SCF-LOSC2. LOSC2 calculation is associated with B3LYP functional. LiH and LiF molecules are stretched at 14 bohr, and HF molecule is stretched at 16 bohr. The Mulliken charge refers to F atom in HF, H atom in LiH and F atom in LiF.

Molecule	SCF-LOSC	macro-SCF-LOSC	Diff (macro - scf)
HF	0.000000	0.000000	0.00E+00
LiH	0.000313	0.000311	-2.00E-06
LiF	0.000310	0.000240	-7.00E-05

same. In the case of stretched LiF, in which the parent functional B3LYP yields delocalized electron density, SCF-LOSC still provide similar results to the ones from macro-SCF-LOSC with the difference of total energy only up to  $1e-4$  a.u. ( $< 0.1$  kcal/mol). Those results indicate the results from the new SCF-LOSC is reliable. Also it suggests that applying macro-SCF-LOSC would not be necessary in practice.

## References

- (S1) An In-House Program for QM/MM Simulations. <https://qm4d.org/>.
- (S2) Gordon, M. S.; Schmidt, M. W. In *Theory and Applications of Computational Chemistry*; Dykstra, C. E., Frenking, G., Kim, K. S., Scuseria, G. E., Eds.; Elsevier: Amsterdam, 2005; pp 1167–1189.
- (S3) Schmidt, M. W.; Baldridge, K. K.; Boatz, J. A.; Elbert, S. T.; Gordon, M. S.; Jensen, J. H.; Koseki, S.; Matsunaga, N.; Nguyen, K. A.; Su, S.; Windus, T. L.; Dupuis, M.; Montgomery, J. A. *J. Comput. Chem.* **1993**, *14*, 1347–1363.
- (S4) Blum, V.; Gehrke, R.; Hanke, F.; Havu, P.; Havu, V.; Ren, X.; Reuter, K.; Scheffler, M. *Comput. Phys. Commun.* **2009**, *180*, 2175–2196.
- (S5) Ren, X.; Rinke, P.; Blum, V.; Wieferink, J.; Tkatchenko, A.; Sanfilippo, A.; Reuter, K.; Scheffler, M. *New J. Phys.* **2012**, *14*, 053020.
- (S6) Frisch, M. J.; Trucks, G. W.; Schlegel, H. B.; Scuseria, G. E.; Robb, M. A.; Cheeseman, J. R.; Scalmani, G.; Barone, V.; Petersson, G. A.; Nakatsuji, H.; Li, X.; Caricato, M.; Marenich, A. V.; Bloino, J.; Janesko, B. G.; Gomperts, R.; Menucci, B.; Hratchian, H. P.; Ortiz, J. V.; Izmaylov, A. F.; Sonnenberg, J. L.; Williams-Young, D.; Ding, F.; Lipparini, F.; Egidi, F.; Goings, J.; Peng, B.; Petrone, A.; Henderson, T.; Ranasinghe, D.; Zakrzewski, V. G.; Gao, J.; Rega, N.; Zheng, G.; Liang, W.; Hada, M.; Ehara, M.; Toyota, K.; Fukuda, R.; Hasegawa, J.; Ishida, M.; Nakajima, T.; Honda, Y.; Kitao, O.; Nakai, H.; Vreven, T.; Throssell, K.; Montgomery, J. A., Jr.; Peralta, J. E.; Ogliaro, F.; Bearpark, M. J.; Heyd, J. J.; Brothers, E. N.; Kudin, K. N.;

Staroverov, V. N.; Keith, T. A.; Kobayashi, R.; Normand, J.; Raghavachari, K.; Rendell, A. P.; Burant, J. C.; Iyengar, S. S.; Tomasi, J.; Cossi, M.; Millam, J. M.; Klene, M.; Adamo, C.; Cammi, R.; Ochterski, J. W.; Martin, R. L.; Morokuma, K.; Farkas, O.; Foresman, J. B.; Fox, D. J. Gaussian 16 Revision A.03. 2016; Gaussian Inc. Wallingford CT.

(S7) Su, N. Q.; Mahler, A.; Yang, W. *J. Phys. Chem. Lett.* **2020**, *11*, 1528–1535.

# Self-consistent calculation of localized orbital scaling correction for correct electron densities and energy level alignment in density functional theory

Yuncai Mei,<sup>†</sup> Zehua Chen,<sup>†</sup> and Weitao Yang<sup>\*,†,‡</sup>

<sup>†</sup>*Department of Chemistry, Duke University, Durham, North Carolina 27708, USA*

<sup>‡</sup>*Department of Physics, Duke University, Durham, North Carolina 27708, USA*

E-mail: weitao.yang@duke.edu

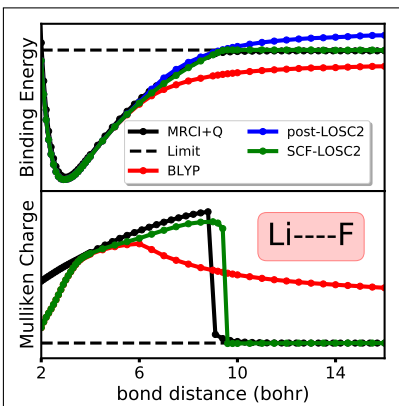
---

<sup>1</sup>Y.M. and Z.C. contributed equally to this paper.

## Abstract

The recently developed localized orbital scaling correction (LOSC) method shows the ability to systematically and size-consistently reduce the delocalization error existing in conventional density functional approximations (DFAs). Applying LOSC to conventional DFAs (LOSC-DFAs) gives much improvement for the description of related properties, including band gaps, total energies and photoemission spectra. However, concern and issue remain: the application of LOSC to DFAs is mainly through a post self-consistent field (SCF) manner, and few results from applying LOSC to DFAs with a SCF manner have been reported. The reason is the originally proposed SCF approach for SCF-LOSC calculation uses an approximate Hamiltonian and encounters convergence problems easily in practice. In this work, we develop a new SCF approach with a correct Hamiltonian and achieve reliable SCF-LOSC calculations. We demonstrate the capability of the new SCF approach for SCF-LOSC to correctly describe the electron densities, total energies and energy level alignment for the molecular dissociation process, while conventional DFAs or LOSC-DFAs with post-SCF calculations show large errors. This work demonstrates that the new SCF approach for SCF-LOSC would be a promising method to study problems for correct electron densities and energy level alignment in large systems.

## Graphical TOC Entry



Density functional theory (DFT)<sup>1-3</sup> has been widely used to calculate and predict the electronic structure of molecular systems in practice. The performance of DFT depends on the quality of applied density functional approximation (DFA) to the exchange-correlation energy  $E_{xc}$ . Although the conventional DFAs, such as local density approximation (LDA),<sup>4,5</sup> general gradient approximations (GGAs)<sup>6-8</sup> and hybrid GGAs,<sup>9-11</sup> are commonly used in practice, they all have the delocalization error<sup>12-15</sup> and fail to describe some critical problems.

The delocalization error in conventional DFAs<sup>12,16</sup> manifests in a size-dependent manner: For small systems, with small number of atoms and having small physical extent, commonly used DFAs have good accuracy describing the total energies of systems with integer number of electrons, but the delocalization error exhibits as the convex deviation from the Perdew-Parr-Levy-Baldurzi (PPLB) linear condition for fractional number of electrons;<sup>17-19</sup> For large systems, with large number of atoms or having large physical extent (as near a dissociation limit), commonly used DFAs have small errors for systems with fractional number of electrons and obey the fractional charge linearity condition at the bulk limit, but the delocalization error reveals as the large errors in total energy for systems with integer number of electrons. Conventional DFAs usually give much lower total energy for the system with fractional charges, making the total energy curve convex for small systems.<sup>18,19</sup> Such delocalization error (convex deviation) leads conventional DFAs to produce large error for the energy derivatives with respect to the electron number, i.e. the chemical potentials,<sup>13,20</sup> leading to underestimation of the exact ionization potentials (IPs) from the HOMO (highest occupied molecular orbital) energies and the overestimation of electron affinities (EAs) from the LUMO (lowest unoccupied molecule orbital) energies. Delocalization error would produce too delocalized electron density, as the error falsely lowers the total energy of the system.<sup>12,14,15</sup> Examples reflecting this issue are the wrong dissociation limits of molecules<sup>21-25</sup> and too low reaction barriers<sup>15</sup> from conventional DFAs. For charge transfer complexes, delocalization error leads to overestimate of charge transfer and the binding energies.<sup>14</sup>

In material interfaces and defects, delocalization error can lead to incorrect charge trans-

fer across the interfaces, and significant error in energy level alignment.<sup>26–29</sup> Interfaces and energy level alignment play important roles in many technological applications: they strongly influence the charge extraction and transport in solar cell devices,<sup>30</sup> and catalysis in semiconductor.<sup>31</sup> Thus it remains an important challenge to describe the correct energy level alignment for interfaces with DFAs.

To reduce the delocalization error, there has been much effort devoted to develop improved functional approximations. These include the development of long-range corrected functionals<sup>32–43</sup> and double hybrid functionals.<sup>44–48</sup> These methods have been shown to reduce delocalization error. But challenges still remain for a systematic correction across system types, sizes and scales.

Recently, our group developed the localized orbital scaling correction (LOSC) method, which imposes the PPLB condition by utilizing orbitalets (a set of molecular orbitals localized on both physical and energy space) to the associated parent DFAs to reduce the delocalization error.<sup>16,49</sup> Benefitting from the novel features of orbitalets that dynamically switch between the canonical orbitals (COs) and localized orbitals (LOs), correction from LOSC can be flexibly and automatically applied on the global or local region of the system. Thus, LOSC shows the ability to reduce the delocalization error in a systematic and size-consistent way. LOSC has been shown to improve greatly the prediction of quasiparticle energies – ionization energies, electron affinities, and also ionized excited state energies for atoms, small molecules and very large systems, all from the eigenvalues of the generalized Kohn-Sham Hamiltonian.<sup>16,49,50</sup> The LOSC prediction accuracy is similar or better than many-electron Green’s function method of GW.<sup>50</sup>

In the original LOSC paper,<sup>16</sup> two approaches for applying LOSC to the parent DFAs have been discussed. One way is in the post self-consistent field manner (post-LOSC), in which the converged electron density from the parent DFA ( $\rho_s^{\text{DFA}}$ ) is directly used to evaluate the energy correction  $\Delta E^{\text{LOSC}}$  from LOSC. The other way is in a self-consistent field manner (SCF-LOSC), in which the LOSC effective Hamiltonian  $\Delta h^{\text{LOSC}} = \frac{\delta \Delta E^{\text{LOSC}}}{\delta \rho_s}$  is



introduced to the DFA Hamiltonian  $h_s^{\text{DFA}}$ . After solving the KS-equations with updated Hamiltonian  $h_s = h_s^{\text{DFA}} + \Delta h^{\text{LOSC}}$  self-consistently, the converged electron density from LOSC-DFA ( $\rho_s^{\text{LOSC-DFA}}$ ) is obtained and the correction  $\Delta E^{\text{LOSC}}$  is therefore evaluated based on  $\rho_s^{\text{LOSC-DFA}}$ . In practice, the originally proposed SCF approach<sup>16</sup> for the SCF-LOSC calculation turns to encounter convergence problems easily, especially for the calculations of large molecules, because only an approximate form of the LOSC effective Hamiltonian has been developed and used. Therefore, only the performance of post-LOSC has been well investigated along the development of LOSC. Although the post-LOSC has been demonstrated to show much improvement to the description of band gaps, total energies and photoemission spectra,<sup>16,49,50</sup> the development of reliable SCF-LOSC approach is still necessary because of the following. First, besides the energetic properties (total energies and orbital energies), the electron density of a molecular system is also an important property, since it closely relates to the molecule’s geometry, chemical bonding and reaction reactivities. The conventional DFAs suffering from the delocalization error can produce much delocalized electron density and underestimate total energy in many cases.<sup>21–25</sup> Applying post-LOSC in these cases is not sufficient because it only improves the energies for the parent DFA but leaves the significant error in electron density unchanged. Second, post-LOSC being an reasonable approximation to the SCF-LOSC is only valid at the condition that  $\rho_s^{\text{DFA}}$  is close to  $\rho_s^{\text{LOSC-DFA}}$ . When  $\rho_s^{\text{DFA}}$  differs much to  $\rho_s^{\text{LOSC-DFA}}$  as the delocalization error from the parent DFA becomes significant, the post-LOSC may not provide reliable results due to the lack of self-consistency, and applying SCF-LOSC calculation becomes necessary.

In this work, we present a new and robust SCF approach to achieve reliable SCF-LOSC calculations. To start, we briefly review the methodology of LOSC. The energy correction from LOSC,  $\Delta E^{\text{LOSC}}$ , is constructed from a set of orbitalets (LOs,  $\{\phi_i\}$ ) those are transformed from the canonical orbitals (COs,  $\{\psi_i\}$ ) by a unitary transformation.  $\Delta E^{\text{LOSC}}$  is expressed as

$$\Delta E^{\text{LOSC}} = \sum_{ij} \frac{1}{2} \kappa_{ij} \lambda_{ij} (\delta_{ij} - \lambda_{ij}), \quad (1)$$

in which  $\kappa$  is the curvature matrix and  $\lambda$  is the local occupation matrix. The curvature matrix shows different expressions in different versions of LOSC. We call the original version of LOSC as LOSC1<sup>16</sup> and the later version as LOSC2<sup>49</sup> in the following text. No matter in which version of LOSC, the curvature matrix is completely and explicitly determined by LOs. For example, the curvature matrix from LOSC1 is defined as

$$\kappa_{ij} = \int \frac{\rho_i(\mathbf{r})\rho_j(\mathbf{r}')}{|\mathbf{r} - \mathbf{r}'|} d\mathbf{r}d\mathbf{r}' - \frac{2\tau C_x}{3} \int [\rho_i(\mathbf{r})]^{\frac{2}{3}} [\rho_j(\mathbf{r})]^{\frac{2}{3}} d\mathbf{r}, \quad (2)$$

where  $\rho_i(\mathbf{r})$  is the local orbital's density and defined as  $\rho_i(\mathbf{r}) = |\phi_i(\mathbf{r})|^2$ . The local occupation matrix  $\lambda$  is completely and explicitly determined by LOs and the KS density operator  $\rho_s$ , and it is expressed as

$$\lambda_{ij} = \langle \phi_i | \rho_s | \phi_j \rangle. \quad (3)$$

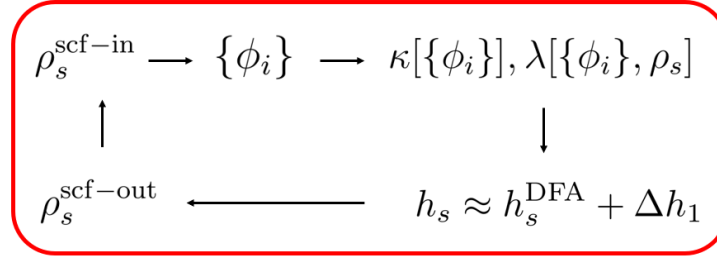


Figure 1: The original SCF procedure with the approximate LOSC effective Hamiltonian.

Figure 1 shows the working flow of the original SCF procedure for SCF-LOSC.<sup>16</sup> In particular, one should notice that both LOs and electron density are updating in every SCF cycle. The dependence of LOs on the electron density in each SCF cycle introduces complexities to derive the exact LOSC effective Hamiltonian. Specifically, according to the original SCF procedure and Eqs. 1 - 3, the exact LOSC effective Hamiltonian  $\Delta h^{\text{LOSC}}$  for the original SCF approach is given by

$$\Delta h^{\text{LOSC}} = \frac{\delta \Delta E[\{\phi_i\}, \rho_s]}{\delta \rho_s} = \frac{\delta \Delta E}{\delta \rho_s} \Big|_{\{\phi_i\}} + \sum_i \frac{\delta \Delta E}{\delta \phi_i} \Big|_{\rho_s} \frac{\delta \phi_i}{\delta \rho_s} + \sum_i \frac{\delta \Delta E}{\delta \phi_i^*} \Big|_{\rho_s} \frac{\delta \phi_i^*}{\delta \rho_s}. \quad (4)$$

The first term (denoted as  $\Delta h_1$ ) on the r.h.s. of Eq. 4 is the explicit contribution with the LOs fixed, and the last two terms (denoted as  $\Delta h_2$ ) are the implicit contribution from the relaxation of LOs with the updating of electron density. Due to the difficulty of evaluating  $\Delta h_2$ , the  $\Delta h_2$  term was ignored in practical calculations. As shown in Figure 1, the LOSC effective Hamiltonian is approximated with only the  $\Delta h_1$  term,

$$\Delta h^{\text{LOSC}} \approx \Delta h_1 = \sum_i \kappa_{ii} \left( \frac{1}{2} - \lambda_{ii} \right) |\phi_i\rangle \langle \phi_i| - \sum_{i \neq j} \kappa_{ij} \lambda_{ij} |\phi_i\rangle \langle \phi_j|. \quad (5)$$

However, such approximate LOSC effective Hamiltonian is not robust in practice, because we find it is easy to cause SCF convergence problem. To solve the convergence problem, one straightforward solution is to derive the  $\Delta h_2$  term to use the exact LOSC effective Hamiltonian. However, this would be complicated and difficult to achieve.

In this paper, we develop an alternative solution to the problem. The idea is to define a new SCF procedure with the removal of LOs' dependence on the electron density in each SCF cycle. The key step is to redefine the LOSC localization procedure, in another word, the localization cost functional. Taking the LOSC2 localization cost functional as an example, the cost functional  $F$  takes the following form,

$$F(\rho_s, \{\psi_i\}, U_{pi}) = (1 - \gamma) \sum_p \left( \langle \mathbf{r}^2 \rangle_p - \langle \mathbf{r} \rangle_p^2 \right) + \gamma C \sum_p \left( \langle h[\rho_s]^2 \rangle_p - \langle h[\rho_s] \rangle_p^2 \right), \quad (6)$$

$$\langle X \rangle_p = \langle \phi_p | X | \phi_p \rangle, \quad X = \mathbf{r}, \mathbf{r}^2, h, h^2, \quad (7)$$

$$\phi_p = \sum_i U_{pi} \psi_i, \quad (8)$$

in which  $U$  is the unitary transformation matrix,  $h$  is the one-electron Hamiltonian of the parent DFA evaluated at the electron density  $\rho_s$  at each SCF cycle, and  $\{\psi_i\}$  are the corresponding COs. Instead of defining the LOSC localization cost functional that is dependent on the electron density and COs in each SCF cycle as shown above, we can just use the electron density  $\rho_s^{\text{DFA}}$  and the corresponding COs  $\{\psi_i^{\text{DFA}}\}$  from a converged DFA calcula-

tion in the cost functional; thus, we obtain a set of predetermined LOs  $\{\phi_i^0\}$  in advance of the SCF-LOSC calculation. Applying this strategy to LO SC2 as an example, the modified localization cost function is expressed as

$$F(\rho_s^{\text{DFA}}, \{\psi_i^{\text{DFA}}\}, U_{pi}) = (1 - \gamma) \sum_p \left( \langle \mathbf{r}^2 \rangle_p - \langle \mathbf{r} \rangle_p^2 \right) + \gamma C \sum_p \left( \langle h[\rho_s^{\text{DFA}}]^2 \rangle_p - \langle h[\rho_s^{\text{DFA}}] \rangle_p^2 \right), \quad (9)$$

$$\langle X \rangle_p = \langle \phi_p^0 | X | \phi_p^0 \rangle, \quad X = \mathbf{r}, \mathbf{r}^2, h, h^2, \quad (10)$$

$$\phi_p^0 = \sum_i U_{pi} \psi_i^{\text{DFA}}, \quad (11)$$

in which  $h$  is now evaluated at the  $\rho_s^{\text{DFA}}$ . Clearly, the LOs in this new SCF approach do not depend on the electron density of each SCF cycle. We keep the same set of LOs  $\{\phi_i^0\}$  during the SCF procedure. This treatment of LOs in the new approach makes the  $\Delta h_2$  term in Eq. 4 vanish and gives the exact LO SC Hamiltonian only with the  $\Delta h_1$  term immediately; that is,

$$\Delta h^{\text{LOSC}} = \frac{\delta \Delta E[\{\phi_i^0\}, \rho_s]}{\delta \rho_s} = \sum_i \kappa_{ii} \left( \frac{1}{2} - \lambda_{ii} \right) |\phi_i^0\rangle \langle \phi_i^0| - \sum_{i \neq j} \kappa_{ij} \lambda_{ij} |\phi_i^0\rangle \langle \phi_j^0|. \quad (12)$$

The LO SC curvature is determined by the set of  $\{\phi_i^0\}$ , and it only needs to be evaluated once. The local occupation matrix is evaluated based on  $\{\phi_i^0\}$  and electron density during the SCF procedure; that is,  $\lambda_{ij} = \langle \phi_i^0 | \rho_s | \phi_j^0 \rangle$ .

The working flow of the new SCF procedure for SCF-LOSC calculation is demonstrated in Figure 2. It involves the following steps: (1) carry out the SCF convergence from the parent DFA to get the converged electron density  $\rho_s^{\text{DFA}}$  and COs  $\{\psi_i^{\text{DFA}}\}$ ; (2) apply the LO SC localization procedure to generate  $\{\phi_i^0\}$  based on  $\rho_s^{\text{DFA}}$  and  $\{\psi_i^{\text{DFA}}\}$ ; (3) construct and store the curvature matrix evaluated from  $\{\phi_i^0\}$ ; (4) use the  $\rho_s^{\text{DFA}}$  as the initial guess to start the SCF-LOSC calculation associated with parent DFA; (5) use the density  $\rho_s$  from current SCF cycle to construct the DFA Hamiltonian  $h_s^{\text{DFA}}$ ; (6) evaluate local occupation matrix based on  $\rho_s$  and  $\{\phi_i^0\}$ , and construct the exact LO SC effective Hamiltonian  $\Delta h^{\text{LOSC}}$  via Eq.

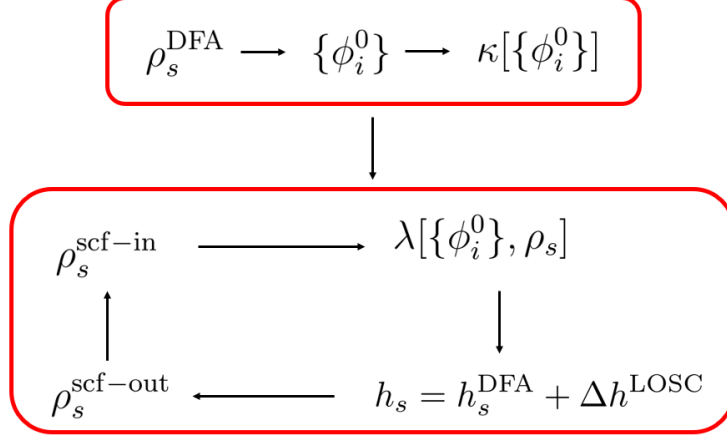


Figure 2: The new SCF procedure with the exact LOSC Hamiltonian.

12; (7) apply  $\Delta h^{\text{LOSC}}$  to  $h_s^{\text{DFA}}$  and update COs and  $\rho_s$ ; (8) check the convergence and go back to step (5) if it is not converged.

In the new SCF-LOSC approach, since the LOSC curvature matrix only needs to be evaluated once and updating the local occupation,  $\lambda_{ij} = \langle \phi_i^0 | \rho_s | \phi_j^0 \rangle$ , is simple, the computational cost for the new SCF-LOSC approach is only about two times that of the conventional DFA SCF calculation. Specifically, one is the generation of LOs from a one-time conventional DFA SCF calculation, and the other is the SCF-LOSC calculation with the corrected KS Hamiltonian, with fixed LOs and LOSC curvature.

Comparing the new SCF approach with the original one, the SCF solution from the new SCF approach may be different from the original SCF-LOSC solution. This is because, at the SCF solution point, the LOs used to evaluate the total energy in the new SCF-LOSC approach are always obtained from  $\rho_s^{\text{DFA}}$ , rather than  $\rho_s^{\text{LOSC-DFA}}$ . The significance of this difference needs to be verified with numerical results. If the relaxation of LOs, like in the original SCF-LOSC, turns to be necessary, we can apply an additional layer of SCF cycle on top of the new SCF-LOSC procedure in order to update the LOs. This two-layer SCF method is noted as macro-SCF-LOSC. Detailed procedure for the macro-SCF-LOSC is described in the supporting information. Ideally, because the macro-SCF-LOSC optimizes both electron density and LOs, the macro-SCF-LOSC should yield the same results as the original SCF-

LOSC approach. From the numerical results shown in the following main text, we find that the macro-SCF-LOSC is not necessary in practice, because the new SCF approach without the macro iteration is already able to provide reliable and excellent results.

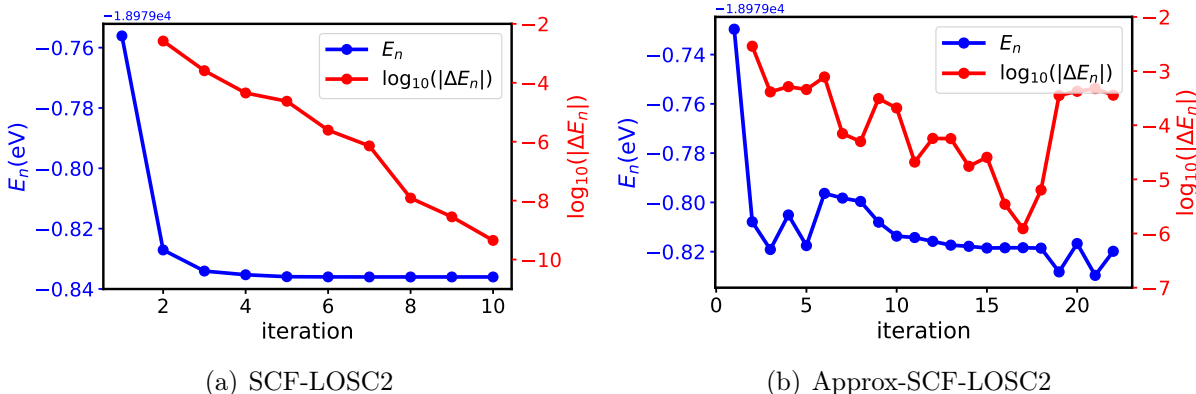


Figure 3: Comparison of SCF performance between (a) SCF-LOSC2 and (b) the original SCF-LOSC2 with approximate Hamiltonian (Approx-SCF-LOSC2) for polyacetylene ( $n = 9$ ).  $E_n$  is the total energy at  $n$ -th iteration step and  $\Delta E_n = E_n - E_{n-1}$ . BLYP is used as the parent functional. 6-31g\* is used as the basis set. aug-cc-pVTZ-RIFIT is used as the density fitting basis in LOSC2 curvature matrix construction.

Now, we check the performance of the new SCF approach for SCF-LOSC calculations. In the following text, the results from SCF-LOSC refer to the new SCF approach, if not specified otherwise. We first study the SCF convergence by testing a long organic molecule, the polyacetylene with 9 units of monomer ( $[\text{C}_2\text{H}_2]_9$ ). As shown in Figure 3, the original SCF approach with the approximate LOSC effective Hamiltonian shows oscillation for total energy along the iterative steps, and it can not reach to the convergence after about 20 steps. The new SCF procedure with the exact LOSC effective Hamiltonian converges smoothly and quickly.

Next, we study the effect of initial guess in the new SCF approach. Note that in step (4) of the new SCF procedure, we use  $\rho_s^{\text{DFA}}$  as the SCF initial guess. This is necessary because the geometric orientation of LOs are fixed in the SCF process. Using  $\rho_s^{\text{DFA}}$  as the initial guess makes sure the orientation of the LOs agree with the one of initial density and initial COs at the beginning. If the used initial electron density has a different orientation than that of

the LOs, it will artificially produce fractional local occupation numbers at the initial step, which may lead the SCF calculation converge to unphysical state with wrong energies. To support the discussion, Table 1 shows results for the test on F atom, with a partially filled p shell. For such small system, the LOs from LO SC localization are just the converged COs from the parent DFA. In other words, the localization is not operative and orbitals are just the COs for small systems. As shown in Table 1, if we use the non-rotated  $\rho_s^{\text{DFA}}$  as the initial guess, the local occupation number will be exact integer (either 1 or 0), and LO SC (both LO SC1 and LO SC2) gives zero correction to the parent DFA. However, if we use the rotated  $\rho_s^{\text{DFA}}$  as the initial guess, which has a set of rotated p orbitals, the fractional local occupation number will be generated artificially and leads non-zero correction to the parent DFA. In the case of LO SC1, we can see such artificial correction is even negative and leads to a unphysical state with energy even lower than DFA. In the case of LO SC2, the artificial energy correction is much smaller. This is because LO SC2 preserves the symmetry much more than LO SC1,<sup>49</sup> making these artificial energy corrections from each fractional local occupation number almost canceled with each other. As a whole, to avoid issues introduced by the orientation of the initial guess, we use the  $\rho_s^{\text{DFA}}$  as the initial guess for the new SCF approach. Note, the choices of LO orientation will not be an issue at all, if the macro-SCF-LO SC is used, because the LO will be generated from  $\rho_s^{\text{LO SC-DFA}}$  in the macro iterations.<sup>51</sup>

With the smooth convergence from the new SCF procedure, we investigate the new SCF-LO SC with the same test sets used in the development of LO SC to test the performance for the atomization energies, reaction barriers, first ionization potentials (IPs) and electron affinities (EAs). Detailed results are documented in the supporting information. In general, the new SCF-LO SC can be conducted easily in these test sets. For the test sets related to atomization energies and reaction barriers, both SCF-LO SC and post-LO SC currently preserve the performance as DFAs. For example, the mean absolute error (MAE) of G2-1 test set for atomization energies is 4.94 kcal/mol for BLYP, and 4.93 kcal/mol for both post-LO SC2-BLYP and SCF-LO SC2-BLYP. The MAE of HTBH38 test case for the reaction

**Table 1: Testing on F atom for the effect of the orientation of initial guess to the new SCF-LOSC approach. BLYP is used as the parent functional. The converged densities from BLYP (rotated/non-rotated) are used as the initial guess. cc-pVTZ is used the basis set. aug-cc-pVTZ-RIFIT is used as the density fitting basis set in LOSC curvature matrix construction. Grid type is (99, 590).**

Method	$E^3$	$\Delta E^4$	$E\_corr(initial)^5$	$E\_corr(SCF)^6$
BLYP	-99.7522856431			
SCF-LOSC1: non-rotated <sup>1</sup>	-99.7522856430	6.31E-11	1.10E-14	1.30E-14
SCF-LOSC1: rotated <sup>2</sup>	-99.7794002845	-2.71E-02	-2.68E-02	-2.71E-02
SCF-LOSC2: non-rotated <sup>1</sup>	-99.7522856430	6.31E-11	1.00E-14	8.00E-15
SCF-LOSC2: rotated <sup>2</sup>	-99.7522340746	5.16E-05	5.27E-05	5.05E-05

<sup>1</sup>The orientation of initial electron density matches to the one of LOs. <sup>2</sup>The orientation of initial electron density does not match to the one of LOs. <sup>3</sup>Total energy. <sup>4</sup>Total energy difference between the SCF-LOSC and BLYP. <sup>5</sup>LOSC energy correction at the first SCF cycle. <sup>6</sup>LOSC energy correction at the last SCF cycle.

barriers is 7.67 kcal/mol for BLYP, 7.49 kcal/mol for post-LOSC2-BLYP, and 7.54 kcal/mol for SCF-LOSC2-BLYP. Such performance is expected because most of cases in these tests are with small molecular sizes and large orbital energy gaps between HOMO and LUMO, which makes orbitals equal to the COs of the parent DFA and the local occupation matrix being diagonal with integer numbers (1 for occupied space and 0 for virtual space). According to energy correction from LOSC shown in Eq. 1, these integer local occupation numbers give zero correction to the total energies. Re-tuning the parameters in the LOSC localization cost function to obtain more balanced localization between the physical space and energy space should provide better performance.<sup>49</sup> However, this task is beyond the scope of current work and will be studied in the future. For the test sets related to IPs and EAs, new SCF-LOSC produces much improvement compared to the parent DFA, and its performance is very similar to the one from post-LOSC for the tested cases. For example, the MAE of IP test set shown in the supporting information is 4.50 eV for BLYP, and 0.62 eV for both post-LOSC2-BLYP and SCF-LOSC2-BLYP.

In the following, we mainly focus on presenting the results that can be significantly different, all related to electron density and energy levels (quasiparticle energies) associated



with the molecular binding/dissociation processes. We first investigate the dissociation of three diatomic molecules (LiF, LiH and HF). B3LYP<sup>6,7,52</sup> is applied as the parent functional, because the SCF convergence from B3LYP can be easily reached at long bond distance for these molecules. Similar GGA calculations would show even larger delocalization error with charge density, but was not obtained because of the SCF failure for large bond lengths. Results from multireference configuration interaction method with the Davidson correction (MRCI+Q)<sup>53-55</sup> are used as the reference and compared to the results from B3LYP, post-LOSC-B3LYP and SCF-LOSC-B3LYP. To study the description of electron density, we look at the Mulliken charges from Mulliken population analysis<sup>56</sup> and the relative total energy of the molecule to its dissociation limit along the dissociation process.

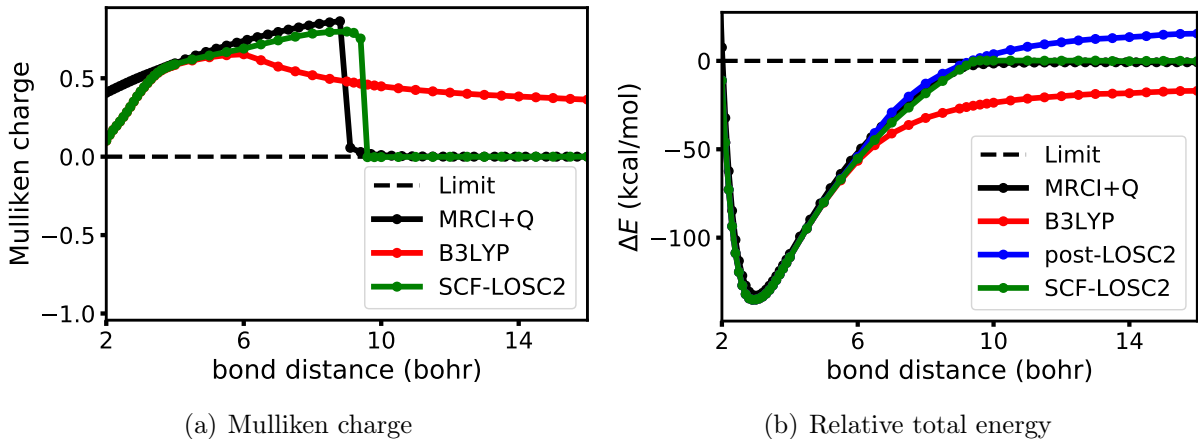


Figure 4: Dissociation of LiF molecule: (a) the Mulliken charge of Li atom; (b) the relative total energy of LiF with respect to Li and F atoms,  $\Delta E = E_{\text{LiF}} - (E_{\text{Li}} + E_{\text{F}})$ . LOSC2 calculations are associated with B3LYP.

Among the three diatomic molecules, B3LYP shows obvious delocalization error for LiF and LiH molecules, making them good cases to demonstrate the performance of the new SCF-LOSC approach. Thus, we highlight the results for LiF and LiH molecules in the main text. Results for HF molecule are documented in the supporting information. The results for LiF are shown in Figure 4. Because  $\text{IP}_{\text{Li}} > \text{EA}_{\text{F}}$ , the LiF molecule must dissociate into neutral Li and F atom (as with all neutral diatomic molecules). Clearly, according to Figure 4, we see B3LYP shows significant delocalization error in electron density, which

is reflected by the positive Mulliken charge of Li atom and underestimated dissociation energy at the dissociation limit. Based on the delocalized electron density from B3LYP, post-LOSC-B3LYP corrects the total energy too much and yields higher dissociation limit. In contrast to the post-LOSC-B3LYP, the SCF-LOSC-B3LYP corrects the electron density. As shown in Figure 4, the Mulliken charge curve from SCF-LOSC-B3LYP matches well with the MRCI+Q reference. In addition, the relative total energy curve from SCF-LOSC-B3LYP almost overlaps with the reference and shows the correct dissociation limit.

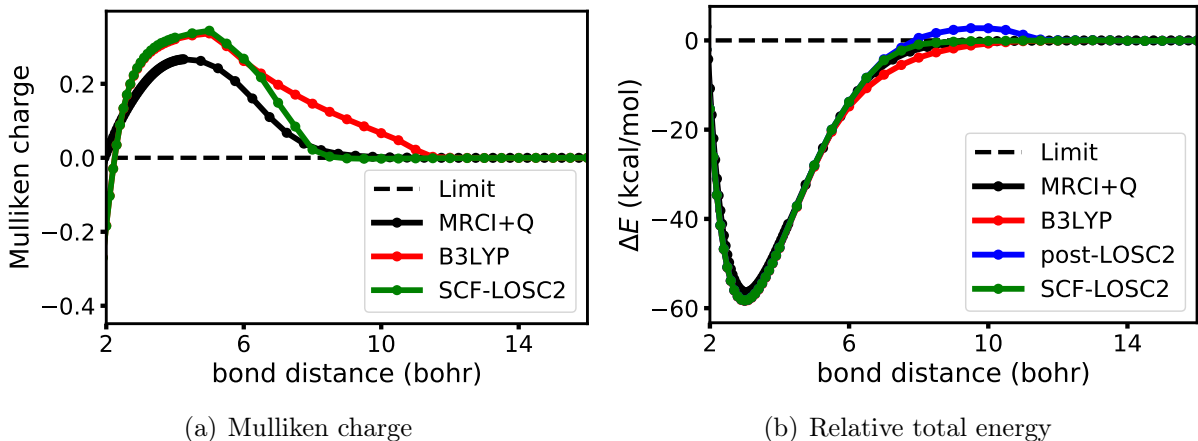


Figure 5: Dissociation of LiH molecule: (a) the Mulliken charge of Li atom; (b) the relative total energy of LiH with respect to Li and H atoms,  $\Delta E = E_{\text{LiH}} - (E_{\text{Li}} + E_{\text{H}})$ . LOSC2 calculations are associated with B3LYP.

Next, we look at the LiH molecule that are shown in Figure 5. Because  $\text{IP}_{\text{Li}} > \text{EA}_{\text{H}}$ , the LiH molecule must dissociate into neutral Li and H atom. According to Figure 5, we notice that although B3LYP gives correct Mulliken charge (zero charge) of Li atom at the dissociation limit, it shows delocalization error at the bond length around 8-10 bohr, in which the MRCI+Q gives almost zero Mulliken charge while B3LYP gives positive charge. Such delocalized electron density (around 8-10 bohr) leads the relative total energy from B3LYP lower than the MRCI+Q reference. In addition, the error in electron density from B3LYP in the range of 8-10 bohr leads the post-LOSC-B3LYP to yield too high relative total energy, showing as the small bump in the dissociation energy curve in Figure 5. From the results of SCF-LOSC-B3LYP, we observe that the electron density is corrected, showing

as the Mulliken charge of Li in the range of 8-10 bohr was corrected down to zero. With the corrected electron density from SCF-LOSC-B3LYP, the relative total energy from SCF-LOSC-B3LYP matches much better with the MRCI+Q reference than B3LYP and post-LOSC-B3LYP.

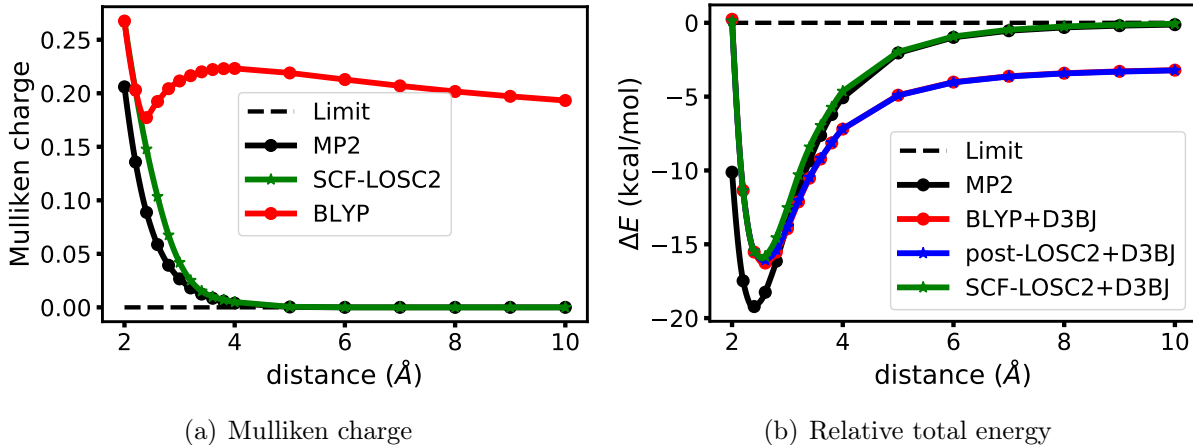


Figure 6: Dissociation of donor-acceptor (D-A) complex (donor: 1,4-benzenediamine, acceptor: tetracyanoethylene (TCNE)) from different methods: (a) the Mulliken charge of the donor molecule; (b) the relative total energy of D-A complex with respect to neutral donor and acceptor molecules,  $\Delta E = E_{DA} - (E_D + E_A)$ . LOSC2 calculations are associated with BLYP. The D3 version of Grimme’s dispersion with Becke-Johnson damping (D3BJ)<sup>57</sup> from BLYP functional is added to all the DFT energy results.

We also study a donor-acceptor (D-A) organic complex system to demonstrate the performance of new SCF-LOSC for more complicated and larger systems. The donor molecule is 1,4-benzenediamine and the acceptor molecule is tetracyanoethylene (TCNE). Because  $IP_D > EA_A$ , the D-A complex will dissociate into two neutral subsystems. Figure 6 shows the Mulliken charge results and the dissociation energy from DFT and MP2<sup>58</sup> calculations. BLYP is used as the parent functional for DFT. Clearly, we see that the parent functional BLYP shows delocalization error at the dissociation limit. The donor molecule has spuriously positive charge, which means there is partial charge transferring from the donor to the acceptor molecule and the electron density is delocalized incorrectly. Due to the delocalized electron density from BLYP, the dissociation energy from BLYP and post-LOSC-BLYP shows similar error. With the correction to the electron density, we see that applying the

new SCF-LOSC gives the right Mulliken charges and total energies along the dissociation coordinates and including dissociation limit.

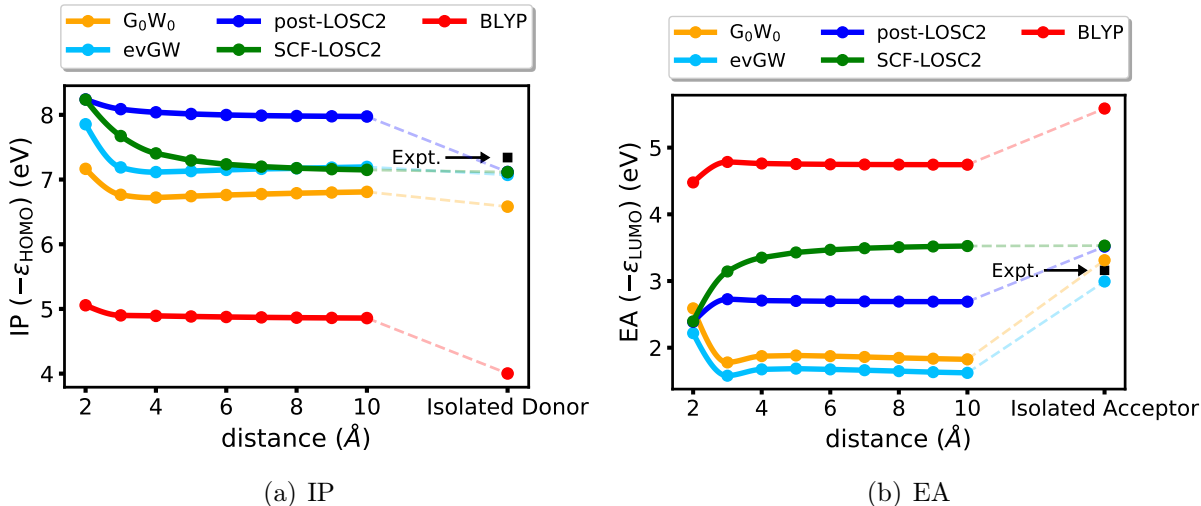


Figure 7: HOMO and LUMO energy level alignment of donor-acceptor (D-A) complex (donor: 1,4-benzenediamine, acceptor: tetracyanoethylene (TCNE)) from different methods: (a) the first IP ( $-\epsilon_{\text{HOMO}}$ ) of D-A complex along the separation distance from 2 to 10 Å. At the right end of the figure, the first IP of the isolated donor molecule is plotted to be compared with the first IP from D-A complex calculations. The experimental IP of the isolated donor molecule is 7.34 eV<sup>59</sup> and marked with an arrow. (b) the first EA ( $-\epsilon_{\text{LUMO}}$ ) of D-A complex along the separation distance from 2 to 10 Å. At the right end of the figure, the first EA of the isolated acceptor molecule is plotted to be compared with the first EA from D-A complex calculations. The experimental EA of the isolated acceptor molecule is 3.16 eV<sup>60</sup> and marked with an arrow. LOSC2 and GW calculations are based on BLYP.

In addition to the Mulliken charge analysis and dissociation energy of this D-A complex system, we examine its energy level alignment (the first IP and EA) along the binding distance. Figure 7 shows the trend of first IP and EA with respect to the change of separation distance. The experimental IP of the donor and EA of the acceptor molecule are plotted as the reference values for the dissociation limit. Along the dissociation, the D-A complex system is calculated with DFT and GW methods (G<sub>0</sub>W<sub>0</sub> and eigenvalue self-consistent GW (evGW)). For the DFT calculations, the negative orbital energy of HOMO and the negative orbital energy of LUMO are used to evaluate the first IP and EA respectively.<sup>61</sup> For GW calculations, the obtained quasiparticle energies are used to evaluate the first IP and EA accordingly. According to Figure 7, we see BLYP shows significant underestimation of IP

and overestimation of EA because of the delocalization error. The results from GW method, which is based on BLYP functional, are also affected by the error in the electron density from BLYP. Especially in the case of EA, the results from GW shows obvious underestimation. At large distances, even at the level of evGW, the error in the EA energy level is underestimated by about 1.5 eV, which is large. Since SCF-LOSC-BLYP corrects the electron density, the results from SCF-LOSC-BLYP are close to the reference value at the dissociation limit, especially for the first IP. The results from post-LOSC-BLYP, shows much improvement compared to the BLYP, however, they are not as good as SCF-LOSC-BLYP results.

The description of interface charge distribution and energy level alignment in this charge transfer system demonstrates the major improvement from the SCF-LOSC and clearly highlights the importance of getting correct charge distributions through self consistent calculations, for the correct energy level alignment in DFT as well as in Green's functional calculations.

In summary, the new SCF-LOSC calculation overcomes the convergence issue and is very effective in practice. More importantly, we observe that the new SCF-LOSC approach is able to produce the correct electron densities, total energies and energy level alignment. The performance from SCF-LOSC is more reliable than the post-LOSC, especially for the cases in which the converged density from the parent DFA shows great delocalization error. With the good performance and reliability, we believe the new SCF-LOSC method would be promising to study problems related to electron densities, and quasiparticle energy level alignment in large molecules and interface systems.

## Acknowledgement

Y. M. and Z.C. acknowledge the support from the National Institute of General Medical Sciences of the National Institutes of Health under award number R01-GM061870. W.Y. acknowledges the support from the National Science Foundation (Grant No. CHE-1900338).

Y. M. was also supported by the Shaffer-Hunnicuttt Fellowship and Z.C. by the Kathleen Zielik Fellowship from Duke University.

## References

- (1) Hohenberg, P.; Kohn, W. Inhomogeneous Electron Gas. *Phys. Rev.* **1964**, *136*, B864–B871.
- (2) Kohn, W.; Sham, L. J. Self-Consistent Equations Including Exchange and Correlation Effects. *Phys. Rev.* **1965**, *140*, A1133–A1138.
- (3) Parr, R. G.; Yang, W. *Density-Functional Theory of Atoms and Molecules*; International Series of Monographs on Chemistry; Oxford University Press: Oxford, New York, 1994.
- (4) Vosko, S. H.; Wilk, L.; Nusair, M. Accurate Spin-Dependent Electron Liquid Correlation Energies for Local Spin Density Calculations: A Critical Analysis. *Can. J. Phys.* **1980**, *58*, 1200–1211.
- (5) Perdew, J. P.; Wang, Y. Accurate and Simple Analytic Representation of the Electron-Gas Correlation Energy. *Phys. Rev. B* **1992**, *45*, 13244–13249.
- (6) Becke, A. D. Density-Functional Exchange-Energy Approximation with Correct Asymptotic Behavior. *Phys. Rev. A* **1988**, *38*, 3098–3100.
- (7) Lee, C.; Yang, W.; Parr, R. G. Development of the Colle-Salvetti Correlation-Energy Formula into a Functional of the Electron Density. *Phys. Rev. B* **1988**, *37*, 785–789.
- (8) Perdew, J. P.; Burke, K.; Ernzerhof, M. Generalized Gradient Approximation Made Simple. *Phys. Rev. Lett.* **1996**, *77*, 3865–3868.

- (9) Stephens, P. J.; Devlin, F. J.; Chabalowski, C. F.; Frisch, M. J. Ab Initio Calculation of Vibrational Absorption and Circular Dichroism Spectra Using Density Functional Force Fields. *J. Phys. Chem.* **1994**, *98*, 11623–11627.
- (10) Adamo, C.; Barone, V. Toward Reliable Density Functional Methods without Adjustable Parameters: The PBE0 Model. *J. Chem. Phys.* **1999**, *110*, 6158–6170.
- (11) Ernzerhof, M.; Scuseria, G. E. Assessment of the Perdew–Burke–Ernzerhof Exchange–Correlation Functional. *J. Chem. Phys.* **1999**, *110*, 5029–5036.
- (12) Mori-Sánchez, P.; Cohen, A. J.; Yang, W. Localization and Delocalization Errors in Density Functional Theory and Implications for Band-Gap Prediction. *Phys. Rev. Lett.* **2008**, *100*, 146401.
- (13) Cohen, A. J.; Mori-Sánchez, P.; Yang, W. Fractional Charge Perspective on the Band Gap in Density-Functional Theory. *Phys. Rev. B* **2008**, *77*, 115123.
- (14) Cohen, A. J.; Mori-Sánchez, P.; Yang, W. Insights into Current Limitations of Density Functional Theory. *Science* **2008**, *321*, 792–794.
- (15) Cohen, A. J.; Mori-Sánchez, P.; Yang, W. Challenges for Density Functional Theory. *Chem. Rev.* **2012**, *112*, 289–320.
- (16) Li, C.; Zheng, X.; Su, N. Q.; Yang, W. Localized Orbital Scaling Correction for Systematic Elimination of Delocalization Error in Density Functional Approximations. *Natl. Sci. Rev.* **2018**, *5*, 203–215.
- (17) Perdew, J. P.; Parr, R. G.; Levy, M.; Balduz, J. L. Density-Functional Theory for Fractional Particle Number: Derivative Discontinuities of the Energy. *Phys. Rev. Lett.* **1982**, *49*, 1691–1694.
- (18) Yang, W.; Zhang, Y.; Ayers, P. W. Degenerate Ground States and a Fractional Number

- of Electrons in Density and Reduced Density Matrix Functional Theory. *Phys. Rev. Lett.* **2000**, *84*, 5172–5175.
- (19) Zhang, Y.; Yang, W. In *Theoretical Chemistry Accounts: New Century Issue*; Cramer, C. J., Truhlar, D. G., Eds.; Springer: Berlin, Heidelberg, 2001; pp 346–348.
- (20) Yang, W.; Cohen, A. J.; Mori-Sánchez, P. Derivative Discontinuity, Bandgap and Lowest Unoccupied Molecular Orbital in Density Functional Theory. *J. Chem. Phys.* **2012**, *136*, 204111.
- (21) Dutoi, A. D.; Head-Gordon, M. Self-Interaction Error of Local Density Functionals for Alkali–Halide Dissociation. *Chem. Phys. Lett.* **2006**, *422*, 230–233.
- (22) Mori-Sánchez, P.; Cohen, A. J.; Yang, W. Many-Electron Self-Interaction Error in Approximate Density Functionals. *J. Chem. Phys.* **2006**, *125*, 201102.
- (23) Ruzsinszky, A.; Perdew, J. P.; Csonka, G. I.; Vydrov, O. A.; Scuseria, G. E. Spurious Fractional Charge on Dissociated Atoms: Pervasive and Resilient Self-Interaction Error of Common Density Functionals. *J. Chem. Phys.* **2006**, *125*, 194112.
- (24) Vydrov, O. A.; Scuseria, G. E.; Perdew, J. P. Tests of Functionals for Systems with Fractional Electron Number. *J. Chem. Phys.* **2007**, *126*, 154109.
- (25) Zheng, X.; Liu, M.; Johnson, E. R.; Contreras-García, J.; Yang, W. Delocalization Error of Density-Functional Approximations: A Distinct Manifestation in Hydrogen Molecular Chains. *J. Chem. Phys.* **2012**, *137*, 214106.
- (26) Flores, F.; Ortega, J.; Vázquez, H. Modelling Energy Level Alignment at Organic Interfaces and Density Functional Theory. *Phys. Chem. Chem. Phys.* **2009**, *11*, 8658–8675.
- (27) Souza, A. M.; Rungger, I.; Pemmaraju, C. D.; Schwingenschloegl, U.; Sanvito, S.



- Constrained-DFT method for accurate energy-level alignment of metal/molecule interfaces. *Phys. Rev. B* **2013**, *88*, 165112.
- (28) Pacchioni, G. First Principles Calculations on Oxide-Based Heterogeneous Catalysts and Photocatalysts: Problems and Advances. *Catal. Lett.* **2015**, *145*, 80–94.
- (29) Egger, D. A.; Liu, Z.-F.; Neaton, J. B.; Kronik, L. Reliable Energy Level Alignment at Physisorbed Molecule–Metal Interfaces from Density Functional Theory. *Nano Lett.* **2015**, *15*, 2448–2455.
- (30) Wang, S.; Sakurai, T.; Wen, W.; Qi, Y. Energy Level Alignment at Interfaces in Metal Halide Perovskite Solar Cells. *Adv. Mater. Interfaces* **2018**, *5*, 1800260.
- (31) Hegner, F. S.; Cardenas-Morcoso, D.; Giménez, S.; López, N.; Galan-Mascaros, J. R. Level Alignment as Descriptor for Semiconductor/Catalyst Systems in Water Splitting: The Case of Hematite/Cobalt Hexacyanoferrate Photoanodes. *ChemSusChem* **2017**, *10*, 4552–4560.
- (32) Savin, A.; Flad, H. Density Functionals for the Yukawa Electron-Electron Interaction. *Int. J. Quantum Chem.* **1995**, *56*, 327–332.
- (33) Gill, P. M. W.; Adamson, R. D.; Pople, J. A. Coulomb-Attenuated Exchange Energy Density Functionals. *Mol. Phys.* **1996**, *88*, 1005–1009.
- (34) Leininger, T.; Stoll, H.; Werner, H.-J.; Savin, A. Combining Long-Range Configuration Interaction with Short-Range Density Functionals. *Chem. Phys. Lett.* **1997**, *275*, 151–160.
- (35) Iikura, H.; Tsuneda, T.; Yanai, T.; Hirao, K. A Long-Range Correction Scheme for Generalized-Gradient-Approximation Exchange Functionals. *J. Chem. Phys.* **2001**, *115*, 3540–3544.

- (36) Toulouse, J.; Colonna, F.; Savin, A. Long-Range-Short-Range Separation of the Electron-Electron Interaction in Density-Functional Theory. *Phys. Rev. A* **2004**, *70*, 062505.
- (37) Yanai, T.; Tew, D. P.; Handy, N. C. A New Hybrid Exchange–Correlation Functional Using the Coulomb-Attenuating Method (CAM-B3LYP). *Chem. Phys. Lett.* **2004**, *393*, 51–57.
- (38) Baer, R.; Neuhauser, D. Density Functional Theory with Correct Long-Range Asymptotic Behavior. *Phys. Rev. Lett.* **2005**, *94*, 043002.
- (39) Vydrov, O. A.; Scuseria, G. E. Assessment of a Long-Range Corrected Hybrid Functional. *J. Chem. Phys.* **2006**, *125*, 234109.
- (40) Vydrov, O. A.; Heyd, J.; Krukau, A. V.; Scuseria, G. E. Importance of Short-Range versus Long-Range Hartree-Fock Exchange for the Performance of Hybrid Density Functionals. *J. Chem. Phys.* **2006**, *125*, 074106.
- (41) Cohen, A. J.; Mori-Sánchez, P.; Yang, W. Development of Exchange-Correlation Functionals with Minimal Many-Electron Self-Interaction Error. *J. Chem. Phys.* **2007**, *126*, 191109.
- (42) Chai, J.-D.; Head-Gordon, M. Systematic Optimization of Long-Range Corrected Hybrid Density Functionals. *J. Chem. Phys.* **2008**, *128*, 084106.
- (43) Baer, R.; Livshits, E.; Salzner, U. Tuned Range-Separated Hybrids in Density Functional Theory. *Annu. Rev. Phys. Chem.* **2010**, *61*, 85–109.
- (44) Zhao, Y.; Lynch, B. J.; Truhlar, D. G. Doubly Hybrid Meta DFT: New Multi-Coefficient Correlation and Density Functional Methods for Thermochemistry and Thermochemical Kinetics. *J. Phys. Chem. A* **2004**, *108*, 4786–4791.

- (45) Grimme, S. Semiempirical Hybrid Density Functional with Perturbative Second-Order Correlation. *J. Chem. Phys.* **2006**, *124*, 034108.
- (46) Chai, J.-D.; Head-Gordon, M. Long-Range Corrected Double-Hybrid Density Functionals. *J. Chem. Phys.* **2009**, *131*, 174105.
- (47) Zhang, Y.; Xu, X.; Goddard, W. A. Doubly Hybrid Density Functional for Accurate Descriptions of Nonbond Interactions, Thermochemistry, and Thermochemical Kinetics. *PNAS* **2009**, *106*, 4963–4968.
- (48) Su, N. Q.; Yang, W.; Mori-Sánchez, P.; Xu, X. Fractional Charge Behavior and Band Gap Predictions with the XYG3 Type of Doubly Hybrid Density Functionals. *J. Phys. Chem. A* **2014**, *118*, 9201–9211.
- (49) Su, N. Q.; Mahler, A.; Yang, W. Preserving Symmetry and Degeneracy in the Localized Orbital Scaling Correction Approach. *J. Phys. Chem. Lett.* **2020**, *11*, 1528–1535.
- (50) Mei, Y.; Li, C.; Su, N. Q.; Yang, W. Approximating Quasiparticle and Excitation Energies from Ground State Generalized Kohn–Sham Calculations. *J. Phys. Chem. A* **2019**, *123*, 666–673.
- (51) see supporting information for more details.
- (52) Becke, A. D. Density-functional Thermochemistry. III. The Role of Exact Exchange. *J. Chem. Phys.* **1993**, *98*, 5648–5652.
- (53) Knowles, P. J.; Werner, H.-J. An Efficient Method for the Evaluation of Coupling Coefficients in Configuration Interaction Calculations. *Chemical Physics Letters* **1988**, *145*, 514–522.
- (54) Langhoff, S. R.; Davidson, E. R. Configuration Interaction Calculations on the Nitrogen Molecule. *Int. J. Quantum Chem.* **1974**, *8*, 61–72.

- (55) Werner, H.-J.; Knowles, P. J. An Efficient Internally Contracted Multiconfiguration–Reference Configuration Interaction Method. *J. Chem. Phys.* **1988**, *89*, 5803–5814.
- (56) Mulliken, R. S. Electronic Population Analysis on LCAO–MO Molecular Wave Functions. I. *J. Chem. Phys.* **1955**, *23*, 1833–1840.
- (57) Grimme, S.; Ehrlich, S.; Goerigk, L. Effect of the Damping Function in Dispersion Corrected Density Functional Theory. *J. Comput. Chem.* **2011**, *32*, 1456–1465.
- (58) Møller, C.; Plesset, M. S. Note on an Approximation Treatment for Many-Electron Systems. *Phys. Rev.* **1934**, *46*, 618–622.
- (59) Streets, D. G.; Elane Hall, W.; Ceasar, G. P. Mesomeric Mixing in the  $\pi$  Energy Levels of Amino-Benzenes Studied by Photoelectron Spectroscopy. *Chem. Phys. Lett.* **1972**, *17*, 90–94.
- (60) Khuseynov, D.; Fontana, M. T.; Sanov, A. Photoelectron Spectroscopy and Photochemistry of Tetracyanoethylene Radical Anion in the Gas Phase. *Chem. Phys. Lett.* **2012**, *550*, 15–18.
- (61) Cohen, A. J.; Mori-Sánchez, P.; Yang, W. Fractional charge perspective on the band gap in density-functional theory. *Phys. Rev. B* **2008**, *77*.